



City Research Online

City, University of London Institutional Repository

Citation: Giaralis, A. and Taflanidis, A. A. (2018). Optimal tuned mass-damper-inerter (TMDI) design for seismically excited MDOF structures with model uncertainties based on reliability criteria. Structural Control & Health Monitoring, 25(2), doi: 10.1002/stc.2082

This is the accepted version of the paper.

This version of the publication may differ from the final published version.

Permanent repository link: <https://openaccess.city.ac.uk/id/eprint/19130/>

Link to published version: <http://dx.doi.org/10.1002/stc.2082>

Copyright: City Research Online aims to make research outputs of City, University of London available to a wider audience. Copyright and Moral Rights remain with the author(s) and/or copyright holders. URLs from City Research Online may be freely distributed and linked to.

Reuse: Copies of full items can be used for personal research or study, educational, or not-for-profit purposes without prior permission or charge. Provided that the authors, title and full bibliographic details are credited, a hyperlink and/or URL is given for the original metadata page and the content is not changed in any way.

Optimal tuned mass-damper-inerter (TMDI) design for seismically excited MDOF structures with model uncertainties based on reliability criteria

A. Giaralis^{a*} and A.A. Taflanidis^b

^aDepartment of Civil Engineering, City, University of London, EC1V 0HB, London, UK

^bDepartment of Civil & Environmental Engineering & Earth Sciences, University of Notre Dame, Notre Dame, IN 46556, USA

SUMMARY

The tuned-mass-damper-inerter (TMDI) is a recently proposed linear passive dynamic vibration absorber for the seismic protection of buildings. It couples the classical tuned-mass-damper (TMD) with an inerter, a two-terminal device resisting the relative acceleration of its terminals, in judicious topologies achieving mass-amplification and higher-modes-damping effects compared to the TMD. This paper considers an optimum TMDI design framework accommodating the above effects while accounting for parametric uncertainty to the host structure properties, modelled as a linear MDOF system, and to the seismic excitation, modelled as stationary colored noise. The inerter device constant, acting as a TMD mass amplifier, is treated as a design variable, while performance variables sensitive to high-frequency structural response dynamics are used to account for the TMDI influence to the higher structural modes. Reliability criteria are adopted for quantifying the structural performance, expressed through the probability of occurrence of different failure modes related to the trespassing of acceptable thresholds for the adopted performance variables: floor accelerations, inter-storey drifts, and attached mass displacement. The design objective function is taken as a linear combination of these probabilities following current performance-based seismic design trends. Analytical and simulation-based tools are adopted for the efficient estimation of the underlying stochastic integral defining the structural performance under uncertainty. A 10-storey building under stationary Kanai-Tajimi stochastic excitation is considered to illustrate the design framework for various TMDI topologies and attached mass values. It is shown that the TMDI achieves enhanced structural performance and robustness to building and excitation uncertainties compared to same mass/weight TMDs.

Keywords: Tuned mass damper inerter; first-passage probability; reliability-based design; parametric uncertainty; stochastic excitation

1. INTRODUCTION

Dynamic vibration absorbers, with main representative the linear tuned mass damper (TMD), have been extensively considered for suppressing vibrations in dynamically excited building structures [1-6]. The TMD consists of a secondary mass attached towards the top of the host or primary structure whose vibration is to be controlled via optimally designed/"tuned" linear spring and dashpot elements. The main design or tuning requirement for the spring coefficient is that the frequency of oscillation of the TMD for a fixed attached mass coincides with the dominant natural frequency of the primary structure, typically the first/fundamental one. This resonance-based design criterion ensures that significant kinetic energy is transferred from the primary structure to the attached mass and is eventually dissipated at the dashpot. To this end, TMD tuning also involves a proper selection of the dashpot coefficient to ensure efficient energy dissipation. Although closed-form expressions for optimum TMD properties (spring and dashpot coefficients) do exist (e.g., [7]), numerical optimization approaches are commonly employed for TMD design. These approaches can accommodate enhanced assumptions for structural performance

* Corresponding author. Senior Lecturer, Department of Civil Engineering, City University London, London, UK. Email: Agathoklis.Giaralis.1@city.ac.uk

quantification and/or the system modeling, such as the use of reliability criteria for evaluating performance [8-10], the explicit consideration of the TMD attached mass displacement (stroke) demand [9], the evaluation of the damper impact over different structural response quantities [10, 11], and the incorporation of uncertainties for the excitation or the structural properties [8, 10]. The latter consideration is quite important in achieving robust TMD designs as the optimal TMD properties rely heavily on the dynamic properties of the primary structure, such as its fundamental natural frequency, which are not usually deterministically known in practical applications.

No matter the adopted tuning approach, the TMD vibration control efficacy and robustness to detuning effects depend on its inertia property; the larger the attached TMD mass that can be accommodated, subject to structural design and architectural constraints, the more effective the TMD will be. This is especially true for seismically excited buildings, for which facilitating a large attached mass becomes a critical parameter in achieving satisfactory performance [12-14]. In this context, various researchers proposed the implementation of unconventionally large-mass TMDs by connecting the top floor, or the last few top floors, to the rest of the building via isolators and, therefore, by treating the top floor(s) of buildings as the “attached” TMD mass [15-17]. In this manner, the TMD mass may reach up to 50% of the total mass of the building or more [12, 16]. However, such “exotic” solutions are not only demanding (and costly) from the structural design and construction viewpoint, but they also add uncertainty and complexity to the optimum TMD design/tuning since under severe ground motions the isolators exhibit non-linear behavior.

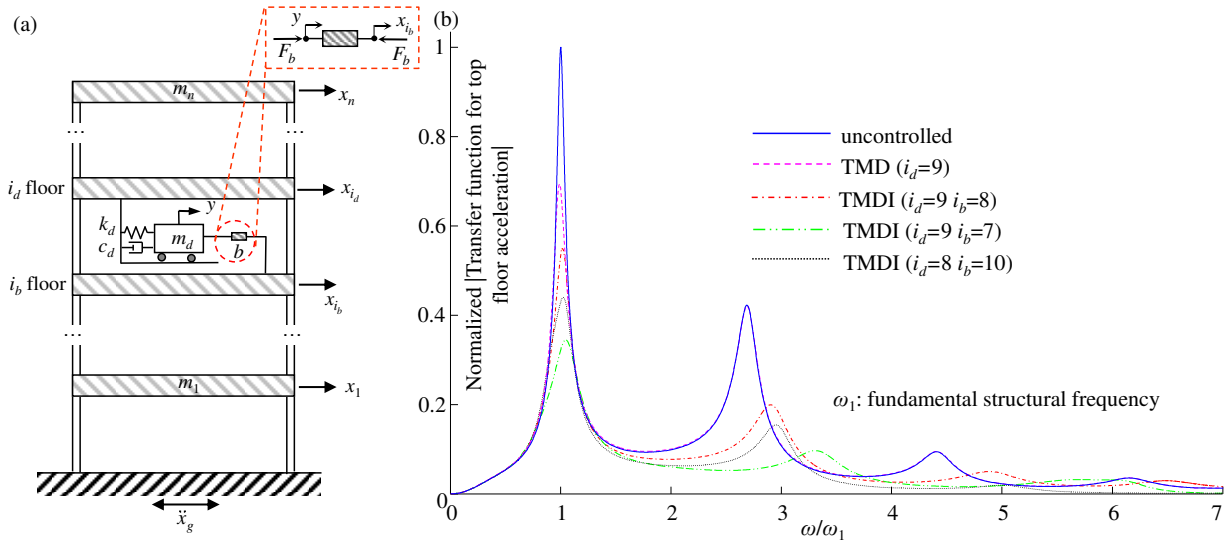


Figure 1: (a) Tuned mass-damper-inerter (TMDI) equipped multi-storey frame structure and ideal inerter device with inertance b under equilibrium with an external force F (inlet); (b) Normalized absolute frequency response functions for the top floor acceleration of the 10-storey structure defined in Section 5.1: uncontrolled structure and structure equipped with three different optimal TMDIs and one optimal TMD with common attached mass equal to 0.5% of the total building mass. Normalization is with respect to the peak value of the uncontrolled structure.

Recognizing the above shortcomings of large-mass TMDs, Marian and Giaralis [18, 19] introduced a generalization of the linear TMD, namely the tuned mass-damper-inerter (TMDI), for

the passive vibration control of earthquake excited multi-storey building structures aiming to achieve enhanced performance compared to a same-mass TMD by exploiting the *mass amplification effect* of the (ideal) inerter. The latter is a linear two-terminal mechanical device of negligible mass/weight developing a resisting force proportional to the relative acceleration of its terminals [20]. The constant of proportionality is termed “inertance” and is measured in mass units (kg). Notably, several different inerter prototypes were devised and experimentally tested over the past decade achieving inertance values orders of magnitude larger than the devices’ physical mass, while observing a linear behavior within relatively wide frequency bands of practical interest [21–24]. These devices are relatively small-scale tailored for and used in vehicle suspension systems. Nevertheless, inerter-like devices and mechanical arrangements, termed inertial or rotational dampers, have been also considered for the seismic protection of building structures either in place of viscous dampers [25], or in conjunction with viscous dampers to enhance their energy dissipation capabilities [26–29]. However, in the TMDI, the inerter is utilized as a mass-amplifier to increase the inertial property of a TMD without increasing its weight [18, 19, 30]. This is achieved by connecting the TMD mass via the inerter to a *different* floor from the one that the TMD is attached to in a multi-storey primary building structure as depicted in Figure 1(a). Specifically, in [18] a particular TMDI topological configuration was examined in which the TMD was located at the top floor and the inerter linked the attached mass to the penultimate floor. For this TMDI topology, it was shown in [19] that for a given primary structure, attached mass, and inertance coefficient an optimally designed TMDI (for spring and dashpot coefficients) can provide significant performance improvement compared to a same-mass optimal TMD in terms of primary structure response displacement variance under stochastic ground excitation.

Besides the mass amplification effect, a more profound implication of the inerter in any TMDI topology is that it influences the dynamics of the primary structure in a wide frequency range and not only at frequencies close to the own TMDI oscillation frequency, as is the case of the classical TMD. This is demonstrated in Figure 1(b) which plots the absolute value of the frequency response function (FRF) of the top floor acceleration of a 10-storey building considered later in the numerical part of the paper. The FRF of the (uncontrolled) primary structure is plotted as well as the FRFs of three different optimally designed TMDI-equipped primary structures with different TMDI topologies and of one optimally designed TMD-equipped structure. Evidently, the TMDI has an important impact on higher modes of vibration and this impact depends significantly on the TMDI topology (i.e., where, along the height of the building, the TMDI mass is attached to and which floor the inerter links this mass to). Notably, a similar higher-mode-influence effect was noted by Lazar et al. [29] for the case of the tuned inerter damper (TID), which can be viewed as a limiting case of a TMDI with zero attached mass. However, in [29] this effect was not accounted for in the TID design, as a tuning approach analogous to Den Hartog [1] classical TMD tuning for harmonic excitation was considered focusing on the maximum amplification factor of the system transfer function. Based on this approach, the authors concluded that placement of the TID to the ground floor achieves optimum vibration suppression in seismically excited multi-storey buildings (see also [31]). More recently, Krenk and Høgsberg [32] presented an integrated approach for the numerical optimization of resonant absorbers with mass or inerter elements corresponding to TMDs or TIDs, respectively. In this approach, the importance of considering the impact of higher

order dynamics was acknowledged, which was approximately considered in the optimum design TMD/TID process through an inertia correction for the quasi-dynamic flexibility properties.

The above discussion suggests that optimum TMDI design for the seismic protection of multi-storey buildings should not focus only on the fundamental mode of the primary structure, as considered in previous studies [18, 19], but, rather, should account for higher order dynamics as well. To accommodate this requirement, a novel optimum TMDI design framework is herein adopted which utilizes first-passage reliability criteria for quantifying performance across different response quantities and uses multiple such quantities in defining the objective function, each having a different behavior in terms of the influence of higher order dynamics. The considered design framework treats the TMD and the TID as special cases of the TMDI and, therefore, establishes a unified optimum design approach for any type of inerter- and/or mass-based dynamic vibration absorber for the seismic protection of multistorey buildings, while it facilitates a seamless comparison among them in achieving optimal performance for a given primary structure. The explicit design of TMDIs (or even TIDs) considering higher mode effects is the first novel contribution of this work. A comparison to simplified design approaches that ignore such effects is also performed, to stress the importance of such a design. Additional contributions include: (i) the robustness of the design and of the performance under parametric uncertainties (for describing structural model and seismic hazard) is examined and important comparisons are drawn between TMDIs and TMDs in terms of that robustness, (ii) the inertance is explicitly treated as a design variable for the TMDI instead of a given properties [19,20], and therefore for a given TMDI topology the mass amplification effect is optimally defined, (iii) different topological configurations are examined for the TMDI and the TID. The latter is supported by an alternative representation of the equations of motion. It should be noted that contribution (i) is seamlessly facilitated through the reliability criteria adopted for evaluating performance across the different considered response quantities. This is another advantage of utilizing first-passage reliability concepts, besides the closer relationship to performance objectives for earthquake engineering applications [33] and the fact that it can explicitly incorporate impact of high order dynamics as deemed essential for the considered application.

Within the adopted framework, the seismic input action is represented by filtered stationary white noise which is a commonly considered approximation of the earthquake excitation in the design of passive control systems (e.g. [33, 34]), especially inertia devices as is the application considered here (e.g [7-10, 19]). The TMDI performance is assessed through the probability of occurrence of different failure modes, calculated analytically as first-passage problem, and the overall design objective is taken as a linear combination of these probabilities, an approach that is well aligned with current practices in performance based earthquake engineering [35]. The impact of parametric modeling uncertainties for the excitation and the structure are also examined and different approaches are discussed for the estimation of the associated probabilistic quantities.

In what follows, the governing equations of motion of a TMDI-equipped multi-storey building are established accommodating any TMDI topology (Section 2), followed (Section 3) by the design problem formulation. Section 4 discusses the evaluation of the objective function, separately for the case with known model characteristics and with parametric model uncertainties in the structure and excitation description. Section 5 then presents a case study for a 10-storey frame structure equipped with TMDIs of different topologies. Comparisons are drawn to the classical TMD, to the TID, to simplified design approaches not accounting for higher-mode

dynamics, as well as among the different TMDI topologies examined with and without parametric model uncertainties. Finally, Section 6 summarizes conclusions and future research.

2. EQUATIONS OF MOTION OF TMDI-EQUIPPED MDOF STRUCTURES

Consider a planar n -storey frame primary structure amenable to be modelled as a lumped-mass damped MDOF system as shown in Figure 1(a). The TMDI consists of a classical TMD located at the i_d -th floor of the primary structure comprising a mass m_d attached to the structure via a linear spring of stiffness k_d and a linear dashpot of damping coefficient c_d . The attached mass is linked to the i_b -th floor by an inerter device of inertance b . Note that for $b=0$ (no inerter) the TMDI coincides with a classical TMD attached to i_d -th floor, while for $m_d=0$ (no mass) the TMDI coincides with the TID in [29] installed in between the i_d -th and the i_b -th floors. In this regard, the herein investigated TMDI can be viewed as a generalization of both the TMD and the TID treated as special cases in the ensuing numerical work.

A convenient formulation of the equations of motion for TMDI-equipped MDOF structures is considered making use of *location* and *connectivity* vectors to enable the study of several different TMDI topologies, as opposed to the single one considered in [18, 19]. Specifically, let $\mathbf{x}_s \in \mathbb{R}^n$ be the vector of floor displacements of the primary structure relative to the ground and $\ddot{\mathbf{x}}_g \in \mathbb{R}$ be the ground acceleration. Denote by $\mathbf{R}_d \in \mathbb{R}^n$ the *TMD location* vector specifying the floor the TMD is attached to (i.e., vector of zeros with a single one in its i_d entry), and by $\mathbf{R}_b \in \mathbb{R}^n$ the *inerter location* vector specifying the floor the inerter is connected to (i.e., vector of zeros with a single one in its i_b entry). Let, also, $y \in \mathbb{R}$ be the displacement of the TMD mass relative to the i_d floor and define the *connectivity* vector by $\mathbf{R}_c = \mathbf{R}_d - \mathbf{R}_b$. Then, the inerter resisting force shown in the inlet of Figure 1(a) can be expressed as $F_b = b(\mathbf{R}_c \dot{\mathbf{x}}_s + \dot{y})$. Further, let $\mathbf{M}_s(\boldsymbol{\theta}_s) \in \mathbb{R}^{n \times n}$, $\mathbf{D}_s(\boldsymbol{\theta}_s) \in \mathbb{R}^{n \times n}$, and $\mathbf{K}_s(\boldsymbol{\theta}_s) \in \mathbb{R}^{n \times n}$ be the mass, damping, and stiffness matrices of the primary structure, respectively, where $\boldsymbol{\theta}_s \in \mathbb{R}^{n_{\theta_s}}$ represents the model parameter vector for the structural model, and denote by $\mathbf{R}_s \in \mathbb{R}^n$ the earthquake influence coefficient vector (vector of ones). Then, the coupled equations of motion for the TMDI equipped structure are written as

$$\begin{aligned} (\mathbf{M}_s(\boldsymbol{\theta}_s) + \mathbf{R}_d m_d \mathbf{R}_d^T + \mathbf{R}_c b \mathbf{R}_c^T) \ddot{\mathbf{x}}_s + (m_d \mathbf{R}_d + b \mathbf{R}_c) \ddot{y} + \mathbf{D}_s(\boldsymbol{\theta}_s) \dot{\mathbf{x}}_s + \mathbf{K}_s(\boldsymbol{\theta}_s) \mathbf{x}_s \\ = -(\mathbf{M}_s(\boldsymbol{\theta}_s) + \mathbf{R}_d m_d \mathbf{R}_d^T) \mathbf{R}_s \ddot{\mathbf{x}}_g, \end{aligned} \quad (1)$$

$$(m_d + b) \ddot{y} + (m_d \mathbf{R}_d^T + b \mathbf{R}_c^T) \ddot{\mathbf{x}}_s + c_d \dot{y} + k_d y = -m_d \mathbf{R}_d^T \mathbf{R}_s \ddot{\mathbf{x}}_g, \quad (2)$$

where the inerter is taken as weightless, similarly to the spring and to the dashpot, and, therefore, it does not attract any horizontal seismic inertial force [19]. Equation (2) suggests that the total inertia of the TMDI is equal to $(m_d + b)$. This observation motivates the definition of the following dimensionless frequency ratio f_d , damping ratio ζ_d , inertance ratio β , and mass ratio μ

$$f_d = \sqrt{\frac{k_d}{(m_d + b)}} / \omega_1; \quad \zeta_d = \frac{c_d}{2(m_d + b)\omega_d}; \quad \beta = \frac{b}{M}; \quad \mu = \frac{m_d}{M} \quad (3)$$

where ω_1 and M is the fundamental natural frequency and the total mass of the primary structure, respectively.

3. DESIGN PROBLEM FORMULATION

3.1 Modeling assumptions and state space description

Let \ddot{x}_g in Eqs. (1) and (2) be a stationary filtered Gaussian white noise stochastic process. A state-space formulation is utilized to determine the response characteristics required in the solution of the optimum TMDI design problem. In this setting, the excitation model is given by

$$\begin{aligned}\dot{\mathbf{x}}_q(t) &= \mathbf{A}_q(\boldsymbol{\theta}_q)\mathbf{x}_q(t) + \mathbf{E}_q w(t) \\ \ddot{x}_g(t) &= \mathbf{C}_q(\boldsymbol{\theta}_q)\mathbf{x}_q(t)\end{aligned}\quad (4)$$

where $w(t) \in \mathbb{R}$ is a zero-mean Gaussian white-noise process with spectral intensity equal to one, $\mathbf{x}_q(t) \in \mathbb{R}^{n_q}$ is the state vector for the excitation, $\mathbf{A}_q(\boldsymbol{\theta}_q) \in \mathbb{R}^{n_q \times n_q}$, $\mathbf{E}_q \in \mathbb{R}^{n_q \times 1}$ and $\mathbf{C}_q(\boldsymbol{\theta}_q) \in \mathbb{R}^{1 \times n_q}$ are the state-space excitation matrices and $\boldsymbol{\theta}_q \in \mathbb{R}^{n_{\theta_q}}$ collects the parameters of the analytically defined excitation filter. Conveniently, the equations of motion of the structural system in Eqs. (1) and (2) can be combined with the excitation model in Eq. (4) in a single excitation/structural system model in state-space written as

$$\begin{aligned}\dot{\mathbf{x}}(t) &= \mathbf{A}(\boldsymbol{\varphi}, \boldsymbol{\theta})\mathbf{x}(t) + \mathbf{E}w(t) \\ \mathbf{z}(t) &= \mathbf{C}(\boldsymbol{\varphi}, \boldsymbol{\theta})\mathbf{x}(t)\end{aligned}\quad (5)$$

where $\mathbf{x}(t) \in \mathbb{R}^{n_x}$ is the state vector, with $n_x = 2n + 2 + n_q$, $\mathbf{z}(t) \in \mathbb{R}^{n_z}$ is the vector of output performance variables with z_i denoting the i^{th} system output component, $\boldsymbol{\theta} = [\boldsymbol{\theta}_s; \boldsymbol{\theta}_q] \in \mathbb{R}^{n_\theta}$ is the augmented model parameter vector, collecting the structural $\boldsymbol{\theta}_s$ (which may include characteristics of the TMDI) and excitation $\boldsymbol{\theta}_q$ model parameters, and $\mathbf{A}(\boldsymbol{\varphi}, \boldsymbol{\theta}) \in \mathbb{R}^{n_x \times n_x}$, $\mathbf{E} \in \mathbb{R}^{n_x \times 1}$ and $\mathbf{C}(\boldsymbol{\varphi}, \boldsymbol{\theta}) \in \mathbb{R}^{n_z \times n_x}$ are the state-space system matrices. Importantly, the matrices $\mathbf{A}(\boldsymbol{\varphi}, \boldsymbol{\theta})$ and $\mathbf{C}(\boldsymbol{\varphi}, \boldsymbol{\theta})$ are functions of both the model parameter vector $\boldsymbol{\theta}$ and of the vector $\boldsymbol{\varphi}$ collecting the controllable (design) parameters of the TMDI, namely c_d , k_d , and b . The derivation of the state space matrices is discussed in Appendix A.

Though a proper selection of the matrix $\mathbf{C}(\boldsymbol{\varphi}, \boldsymbol{\theta})$ the state-space formulation in Eq.(5) can be used to determine the statistics of any response quantity expressed as a linear combination of the state vector \mathbf{x} , such as modal response characteristics, inter-storey drifts and floor accelerations, as detailed in the following sub-section. In doing so, the effect of the spectral characteristics of the stochastic excitation governed by the $\boldsymbol{\theta}_q$ parameters is explicitly taken into account.

3.2 Response statistics determination

For a given $\boldsymbol{\theta}$ vector (either deterministically known or sampled from a distribution function in accounting for model uncertainty as discussed later), the output vector $\mathbf{z}(t)$ of the linear system in Eq. (5) exposed to stationary white Gaussian zero-mean noise $w(t)$ follows a Gaussian distribution with zero-mean and stationary covariance matrix

$$\mathbf{K}_{zz}(\boldsymbol{\varphi}, \boldsymbol{\theta}) = \mathbf{C}(\boldsymbol{\varphi}, \boldsymbol{\theta})\mathbf{P}(\boldsymbol{\varphi}, \boldsymbol{\theta})\mathbf{C}(\boldsymbol{\varphi}, \boldsymbol{\theta})^T. \quad (6)$$

In the above equation, the state covariance matrix, $\mathbf{P}(\boldsymbol{\varphi}, \boldsymbol{\theta})$, is determined by the solution of the following Lyapunov equation [36]

$$\mathbf{A}(\boldsymbol{\varphi}, \boldsymbol{\theta})\mathbf{P}(\boldsymbol{\varphi}, \boldsymbol{\theta}) + \mathbf{P}(\boldsymbol{\varphi}, \boldsymbol{\theta})\mathbf{A}(\boldsymbol{\varphi}, \boldsymbol{\theta})^T + \mathbf{E}\mathbf{E}^T = \mathbf{0}. \quad (7)$$

The variance of each of the n_z system output variables $z_i = \mathbf{n}_i^T \mathbf{z}$ ($i=1, 2, \dots, n_z$) is given as

$$\sigma_{z_i}^2(\boldsymbol{\varphi} | \boldsymbol{\theta}) = \mathbf{n}_i^T \mathbf{C}(\boldsymbol{\varphi}, \boldsymbol{\theta}) \mathbf{P}(\boldsymbol{\varphi}, \boldsymbol{\theta}) \mathbf{C}(\boldsymbol{\varphi}, \boldsymbol{\theta})^T \mathbf{n}_i, \quad (8)$$

where the notation “|” is used to stress out that the response variances are functions of both the design vector $\boldsymbol{\varphi}$ and the model parameter vector $\boldsymbol{\theta}$ and \mathbf{n}_i is a n_z dimensional vector with zeros with the i_{th} component being one. Further, in evaluating the reliability (i.e., survival probability) of the response quantities z_i required in the optimum TMDI design problem presented in the following sub-section, the variance of the first time derivative of z_i needs to be computed. This is achieved by using the expression

$$\sigma_{\dot{z}_i}^2(\boldsymbol{\varphi} | \boldsymbol{\theta}) = \mathbf{n}_i^T \mathbf{C}(\boldsymbol{\varphi}, \boldsymbol{\theta}) \mathbf{A}(\boldsymbol{\varphi}, \boldsymbol{\theta}) \mathbf{P}(\boldsymbol{\varphi}, \boldsymbol{\theta}) \mathbf{A}(\boldsymbol{\varphi}, \boldsymbol{\theta})^T \mathbf{C}(\boldsymbol{\varphi}, \boldsymbol{\theta})^T \mathbf{n}_i \quad (9)$$

which is derived under the condition $\mathbf{C}(\boldsymbol{\varphi}, \boldsymbol{\theta}) \mathbf{E} = 0$. The latter condition is necessary to ensure that the out-crossing rate of the z_i stochastic process is finite [33]. Lastly, the frequency response function of z_i , also required in the calculation of the out-crossing rate of z_i , is given by

$$H_{z_i}(\omega | \boldsymbol{\varphi}, \boldsymbol{\theta}) = \mathbf{n}_i^T \mathbf{C}(\boldsymbol{\varphi}, \boldsymbol{\theta}) [j\omega \mathbf{I}_{n_x} - \mathbf{A}(\boldsymbol{\varphi}, \boldsymbol{\theta})]^{-1} \mathbf{E}, \quad (10)$$

3.3 TMDI design using first-passage reliability criteria

In this work, criteria quantified through the first-passage reliability of individual response quantities are used to determine the optimum TMDI design variable vector $\boldsymbol{\varphi}$ accounting for uncertainty to the model parameter vector $\boldsymbol{\theta}$ which contains both excitation and structural properties. Specifically, the the probability that each output (performance) variable z_i in Eq.(5) exceeds a given threshold β_i (defining acceptable performance) within some time-window T of the excitation (strong ground motion duration) is utilized. This probability is quantified as

$$P_i(\boldsymbol{\varphi} | T) = P \left[|z_i(\tau)| > \beta_i \text{ for some } \tau \in [0, T] \right] \quad (11)$$

where $P[\cdot]$ stands for probability. The overall design objective function is taken as a combination of these different probabilities over all the monitored performance variables n_z . That is,

$$J(\boldsymbol{\varphi}) = \sum_{i=1}^{n_z} w_i P_i(\boldsymbol{\varphi} | T), \quad (12)$$

where w_i are weights representing the relative consequences for each failure mode $|z_i| > \beta_i$. The optimal TMDI parameters are then obtained through the optimization problem

$$\boldsymbol{\varphi}^* = \arg \min_{\boldsymbol{\varphi} \in \Phi} J(\boldsymbol{\varphi}), \quad (13)$$

where Φ corresponds to the admissible design space.

To this end, it is important to note that the common optimum design approaches for the classical TMD focus only on the fundamental response mode (e.g. [4, 9]). This is because the TMD can only suppress the primary structure response within a narrow frequency band (close to its frequency of oscillation). However, as discussed in the introduction, the TMDI alters the primary structure response over a wide frequency range and this should be accounted for in the optimum design. This requirement can be readily accomplished by the herein proposed optimum TMDI design formulation by considering performance variables z_i with sensitivity to higher-order-dynamics (i.e., high frequencies and therefore higher-modes) such as the floor acceleration response. Nevertheless, note that even if a single performance variable is considered in the optimization, the objective function in Eq. (12) coupled with the state-space approach for the

calculation of response statistics will account for the response vibration characteristics over the entire frequency domain; state-space analysis incorporates no modal truncation (all modes considered) whereas the outcrossing rate involved in the failure probability (see details in next section) considers the overall response, not constrained around some specific frequency range/mode. In addition, the performance quantification in Eqs. (12) and (11) can seamlessly address modeling uncertainties as will be detailed in Section 4.

Some further discussion is also warranted about how the objective function in Eq. (12) compares to other reliability-based design approaches that have been considered for structural control applications in a similar setting [33, 37] (i.e., stationary excitation and multiple performance variables describing system response). Such studies have adopted a traditional reliability-based design framework, defining the objective function to correspond to the intersection of the different failure modes (i.e., “series” system configuration for defining first-passage reliability). However, the herein proposed approach considers the contribution of each of the individual failure modes separately (upon weighting), which is better aligned with current performance based earthquake engineering practices [35, 38], that add the contributions from all the examined damage states. As will be shown in Section 4 the aforementioned reliability-based approaches lead to equivalent expressions as in Eq. (12), but with the weight w_i replaced by a term that accounts for correlation between the failure modes [39]. In the proposed approach these weights should be interpreted, instead, as consequence weightings, distinguishing the importance of occurrence of different failure modes.

In solving the design problem in Eq.(13), the evaluation of the probabilities $P_i(\boldsymbol{\varphi}|T)$ is conditioned on prior knowledge or assumptions of the system model. In case that all model parameters $\boldsymbol{\theta}$ are deterministically known, the only uncertainty in the system model stems from the random input $w(t)$. On the other hand, if there is uncertainty in the $\boldsymbol{\theta}$ values, then this additional uncertainty affects $P_i(\boldsymbol{\varphi}|T)$ and should be accounted for. These two instances are separately addressed in the next section discussing the solution of the optimization in Eq.(13).

4. SOLUTION OF THE DESIGN PROBLEM

4.1 Deterministic system parameters

For a deterministically defined parameter vector $\boldsymbol{\theta}$, the probability $P_i(\boldsymbol{\varphi}|T) = P_i(\boldsymbol{\varphi}|T, \boldsymbol{\theta})$ corresponds to the first-passage probability for output z_i out-crossing threshold β_i . Under the stationarity assumption, this probability is approximated by

$$P_i(\boldsymbol{\varphi}|T, \boldsymbol{\theta}) = 1 - e^{-\nu_i^+(\boldsymbol{\varphi}|\boldsymbol{\theta})T} \quad (14)$$

where $\nu_i^+(\boldsymbol{\varphi}|\boldsymbol{\theta})$ is the conditional out-crossing rate for z_i given as [39]

$$\nu_i^+(\boldsymbol{\varphi}|\boldsymbol{\theta}) = \lambda_i(\boldsymbol{\varphi}|\boldsymbol{\theta})r_i^+(\boldsymbol{\varphi}|\boldsymbol{\theta}), \quad (15)$$

that is, as a product of two factors: the Rice’s unconditional out-crossing rate $r_i^+(\boldsymbol{\varphi}|\boldsymbol{\theta})$, and the temporal-correlation correction factor $\lambda_i(\boldsymbol{\varphi}|\boldsymbol{\theta})$. The former factor is given by [40]

$$r_i^+(\boldsymbol{\varphi}|\boldsymbol{\theta}) = \frac{\sigma_{z_i}(\boldsymbol{\varphi}|\boldsymbol{\theta})}{\pi\sigma_{z_i}(\boldsymbol{\varphi}|\boldsymbol{\theta})} e^{-\frac{\beta_i^2}{2\sigma_{z_i}^2(\boldsymbol{\varphi}|\boldsymbol{\theta})}} \quad (16)$$

in which the required variances can be computed by Eqs. (8) and (9). This rate assumes independence between out-crossing events for the process z_i . The temporal correlation factor $\lambda_i(\boldsymbol{\varphi}|\boldsymbol{\theta})$ is utilized as a heuristic “correction factor” aiming to approximately address errors introduced by the above independence assumption. This factor is important for problems involving narrow-band systems or in cases where out-crossing of threshold β_i is a frequent event [39]. From the various semi-empirical expressions proposed in the literature, the correction factor proposed in [39] (see references therein for alternative options) is adopted here as it was proved accurate for systems with important higher order dynamics. This factor is given by

$$\lambda_i(\boldsymbol{\varphi}|\boldsymbol{\theta}) \approx \frac{1 - \exp\left\{-q(\boldsymbol{\varphi}|\boldsymbol{\theta})^{0.6} \left(\frac{2}{\sqrt{\pi}}\right)^{0.1} \frac{\beta_i \sqrt{2}}{\sigma_{z_i}(\boldsymbol{\varphi}|\boldsymbol{\theta})}\right\}}{1 - \exp\left\{-\frac{\beta_i^2}{2\sigma_{z_i}^2(\boldsymbol{\varphi}|\boldsymbol{\theta})}\right\}}, \quad (17)$$

where for a process with spectral density function $S_{z_i z_i}(\omega|\boldsymbol{\varphi}, \boldsymbol{\theta})$

$$q(\boldsymbol{\varphi}|\boldsymbol{\theta}) = \frac{\sigma_{z_i}^6(\boldsymbol{\varphi}|\boldsymbol{\theta})}{4\pi \int_{-\infty}^{\infty} |\omega| S_{z_i z_i}(\omega|\boldsymbol{\varphi}, \boldsymbol{\theta}) d\omega \int_{-\infty}^{\infty} S_{z_i z_i}^2(\omega|\boldsymbol{\varphi}, \boldsymbol{\theta}) d\omega}. \quad (18)$$

For the calculation of the integrals in the denominator of Eq. (18), the spectral density $S_{z_i z_i}(\omega|\boldsymbol{\varphi}, \boldsymbol{\theta})$ is substituted by the equivalent expression

$$S_{z_i z_i}(\omega|\boldsymbol{\varphi}, \boldsymbol{\theta}) = |H_{z_i}(\omega|\boldsymbol{\varphi}, \boldsymbol{\theta})|^2 \quad (19)$$

with $H_{z_i}(\omega|\boldsymbol{\varphi}, \boldsymbol{\theta})$ given by Eq. (10). The frequency range over which the system dynamics are important is partitioned at desired points and the frequency response is calculated. The one-dimensional integral is then evaluated via standard numerical integration.

Substituting Eq. (14) in Eq. (12) leads to the following expression for the objective function

$$J(\boldsymbol{\varphi}|\boldsymbol{\theta}) = \sum_{i=1}^{n_z} w_i P_i(\boldsymbol{\varphi}|T, \boldsymbol{\theta}) = \sum_{i=1}^{n_z} w_i \left[1 - e^{-\nu_i^+(\boldsymbol{\varphi}|\boldsymbol{\theta})T}\right]. \quad (20)$$

The optimization problem of Eq. (13) can then be solved by using any appropriate nonlinear optimization algorithm to obtain the *nominal design* solution $\boldsymbol{\varphi}_n^*$

$$\boldsymbol{\varphi}_n^* = \arg \min_{\boldsymbol{\varphi} \in \mathcal{D}} J(\boldsymbol{\varphi}|\boldsymbol{\theta}). \quad (21)$$

To gain a further insight into the design problem at hand, a Taylor series expansion may be used to approximate the quantity in the brackets in Eq. (20). By maintaining only the first expansion term, an accurate approximation of the objective function in Eq.(20) is obtained for cases in which the product $\nu_i^+(\boldsymbol{\varphi}|\boldsymbol{\theta})T$ attain a relatively small value [37] as in

$$J(\boldsymbol{\varphi}|\boldsymbol{\theta}) \approx T \sum_{i=1}^{n_z} w_i \nu_i^+(\boldsymbol{\varphi}|\boldsymbol{\theta}) = T \sum_{i=1}^{n_z} w_i \lambda_i(\boldsymbol{\varphi}|\boldsymbol{\theta}) r_i^+(\boldsymbol{\varphi}|\boldsymbol{\theta}), \quad (22)$$

where Eq. (15) has been substituted for the out-crossing rate in the second equality. This approximation shows that the duration T has a small influence on the problem formulation. Furthermore, it is seen that, from the design optimization viewpoint, the contribution of $\lambda_i(\boldsymbol{\varphi}|\boldsymbol{\theta})$ is not significant since, as discussed earlier, this factor becomes important for relatively lightly-

damped systems, which, with the inclusion of the TMDI, it is not expected to be the case in the considered system. However, the Rice's out-crossing rate, $r_i^+(\boldsymbol{\varphi}|\boldsymbol{\theta})$, contribution is essential since it is directly related to the "failure events," i.e., the out-crossing of the β_i thresholds. Focusing on on Eq.(16), it is seen that this rate is a product of an exponential term, which increases with the variance $\sigma_{z_i}^2(\boldsymbol{\varphi}|\boldsymbol{\theta})$, and of the factor $\sigma_{z_i}^2(\boldsymbol{\varphi}|\boldsymbol{\theta})/\sigma_{z_i}^2(\boldsymbol{\varphi}|\boldsymbol{\theta})$ which increases with the bandwidth of z_i [41]. In this regard, the variance $\sigma_{z_i}^2(\boldsymbol{\varphi}|\boldsymbol{\theta})$ is numerically the most important component for the optimization, since Rice's rate is more sensitive to changes in this variance which enters the exponent in Eq.(16) than to the bandwidth.

Notably, Eq. (22) facilitates a comparison to previous studies which examined the intersection of failure modes in defining the objective function [33, 37] (i.e. series system configuration). In these studies, an expression similar to Eq. (22) was established with a spatial-correlation factor assigned, though, to each variable z_i , in place of the weights w . As detailed in [39] this factor ultimately accounts for the correlation between the failure modes. This practice yields reduced weights to failure modes whose occurrence is highly correlated to a previous out-crossing of some other failure mode. However, the current approach enables the contributions from all failure modes to be weighted judiciously based on application-dependent practical considerations within a performance-based earthquake engineering context.

4.2 Uncertainty in model description

Suppose that uncertainty is involved in the model description quantified by a probability distribution function (pdf), $p(\boldsymbol{\theta})$, to describe the relative plausibility of different model parameter values $\boldsymbol{\theta}$. This pdf ultimately incorporates the available knowledge, expressed in statistical/probabilistic terms, about the structural model and the excitation into the design problem. Using the total probability theorem the failure probability $P_i(\boldsymbol{\varphi}|T)$ is evaluated as

$$P_i(\boldsymbol{\varphi}|T) = \int_{\Theta} P_i(\boldsymbol{\varphi}|T, \boldsymbol{\theta}) p(\boldsymbol{\theta}) d\boldsymbol{\theta}, \quad (23)$$

where Θ corresponds to the region of possible values for $\boldsymbol{\theta}$ and the first-passage probability $P_i(\boldsymbol{\varphi}|T, \boldsymbol{\theta})$ is given by Eq. (14). The objective function for *robust design* is then transformed to

$$J(\boldsymbol{\varphi}) = \sum_{i=1}^{n_z} w_i P_i(\boldsymbol{\varphi}|T) = \sum_{i=1}^{n_z} w_i \int_{\Theta} P_i(\boldsymbol{\varphi}|T, \boldsymbol{\theta}) p(\boldsymbol{\theta}) d\boldsymbol{\theta} = \int_{\Theta} \sum_{i=1}^{n_z} w_i P_i(\boldsymbol{\varphi}|T, \boldsymbol{\theta}) p(\boldsymbol{\theta}) d\boldsymbol{\theta}. \quad (24)$$

By defining consequence measure $k(\boldsymbol{\varphi}|\boldsymbol{\theta})$ as

$$k(\boldsymbol{\varphi}|\boldsymbol{\theta}) = \sum_{i=1}^{n_z} w_i P_i(\boldsymbol{\varphi}|T, \boldsymbol{\theta}) = \sum_{i=1}^{n_z} w_i \left[1 - e^{-v_i^+(\boldsymbol{\varphi}|\boldsymbol{\theta})T} \right], \quad (25)$$

the robust objective function can be simply written as its expected value under distribution $p(\boldsymbol{\theta})$

$$J(\boldsymbol{\varphi}) = \int_{\Theta} k(\boldsymbol{\varphi}|\boldsymbol{\theta}) p(\boldsymbol{\theta}) d\boldsymbol{\theta} \quad (26)$$

Hence, the solution of the robust design problem involves the estimation of the multi-dimensional probabilistic integral in Eq. (26) and two approaches are discussed next for this task.

4.2.1 Estimation of the probabilistic integral

The first approach for estimating the integral of Eq. (26) is based on the asymptotic approximation for integrals of this type developed by Papadimitriou et al. [42]. This ultimately entails fitting a scaled Gaussian function over the logarithm of the integrand around its design

point where the global maximum is attained. The original integral is then approximated by the integral corresponding to this fitted function, leading to the approximation

$$J(\boldsymbol{\varphi}) \approx (2\pi)^{n_\theta/2} \frac{k(\boldsymbol{\varphi} | \boldsymbol{\theta}^*) p(\boldsymbol{\theta}^*)}{\sqrt{|\mathbf{H}_s(\boldsymbol{\theta}^* | \boldsymbol{\varphi})|}}, \quad (27)$$

where $\boldsymbol{\theta}^*$ is the design point for the integrand

$$\boldsymbol{\theta}^* = \arg \max_{\boldsymbol{\theta} \in \Theta} [k(\boldsymbol{\varphi} | \boldsymbol{\theta}) p(\boldsymbol{\theta})], \quad (28)$$

and $\mathbf{H}_s(\boldsymbol{\theta} | \boldsymbol{\varphi}) = \nabla_{\boldsymbol{\theta}} \nabla_{\boldsymbol{\theta}} [\log\{k(\boldsymbol{\varphi} | \boldsymbol{\theta}) p(\boldsymbol{\theta})\}]$ is the Hessian of the logarithm of the integrand with respect to $\boldsymbol{\theta}$ which needs to be numerically evaluated. The estimation of Eq. (27) involves small computational effort, especially if the dimension of $\boldsymbol{\theta}$ is small (below 5-10 model parameters), but its accuracy is unknown and depends on how well the actual integrand is approximated by the fitted Gaussian. In a number of studies [39, 42, 43] this approximation has been demonstrated to yield good accuracy for applications similar to the one examined here. For cases for which optimization of Eq. (28) yields multiple local minima (i.e. multiple design points), then the analytical approximation of Eq. (27) can be established by summing the contribution of the scaled Gaussian functions fitted over each of them, weighted by appropriate reduction factors that take into account the potential overlapping between these functions [44].

The second approach for estimation of the integral of Eq. (26) is based on stochastic (Monte Carlo) simulation. In this case an unbiased estimate is obtained and the accuracy of that estimate can be controlled by the number of samples utilized [45]. This accuracy can be further increased by using importance sampling (IS). The idea behind IS is to introduce an auxiliary density $q(\boldsymbol{\theta})$ so that the computational effort in the stochastic simulation is concentrated in regions of Θ that have higher contribution to the integrand of the probabilistic integral. Using N samples, $\{\boldsymbol{\theta}^j; j=1, \dots, N\}$ from the density $q(\boldsymbol{\theta})$ an estimate for $J(\boldsymbol{\varphi})$ is obtained as

$$J(\boldsymbol{\varphi}) \approx \frac{1}{N} \sum_{i=1}^N k(\boldsymbol{\varphi} | \boldsymbol{\theta}^j) \frac{p(\boldsymbol{\theta}^j)}{q(\boldsymbol{\theta}^j)}. \quad (29)$$

Even for cases where multiple design points exist, the estimate in Eq. (29) yields a good approximation [43] if $q(\boldsymbol{\theta})$ is chosen such that its peak is near a prominent design point and has a spread as large as $p(\boldsymbol{\theta})$. Note that if information about multiple design points is available then it can be used to select more efficient densities, for example a Gaussian mixture. Overall, the stochastic simulation approach provides a more robust estimate for the probabilistic-integral representing $J(\boldsymbol{\varphi})$, but, typically, at a higher computational cost compared to the analytic expansion in Eq. (27). However, if the dimension n_θ of the model parameter vector $\boldsymbol{\theta}$ is high (over 20-30 variables) then the computational cost for the analytic expansion, involving a sufficient number of evaluations of $k(\boldsymbol{\varphi} | \boldsymbol{\theta})$ for numerically estimating the design point and the Hessian, is expected to be comparable to the computational cost for an accurate integral estimation by stochastic simulation. For lower valued of n_θ the analytic expansion is expected to be more computationally efficient.

4.2.2 Design optimization

For solving the robust design problem an efficient two-stage approach is adopted here. In the first stage the analytic expansion is adopted, leading to the simultaneous optimization for the design points and the optimal design variables

$$\begin{aligned}\boldsymbol{\theta}^* &= \arg \max_{\boldsymbol{\theta} \in \Theta} [k(\boldsymbol{\varphi} | \boldsymbol{\theta}) p(\boldsymbol{\theta})] \\ \boldsymbol{\varphi}^* &= \arg \min_{\boldsymbol{\varphi} \in \Phi} \left[(2\pi)^{n_{\theta}/2} \frac{k(\boldsymbol{\varphi} | \boldsymbol{\theta}^*) p(\boldsymbol{\theta}^*)}{\sqrt{|\mathbf{H}_s(\boldsymbol{\theta}^* | \boldsymbol{\varphi})|}} \right]\end{aligned}\quad (30)$$

Once this stage has converged a refinement of the identified optimum is obtained using stochastic simulation to calculate the objective function (facilitating higher accuracy). An IS proposal density, $q(\boldsymbol{\theta})$, is established utilizing the information for the design point $\boldsymbol{\theta}^*$ at the optimal design configuration from the first stage $\boldsymbol{\varphi}^*$ (facilitating higher efficiency in the stochastic simulation). This density then supports the simulation-based optimization

$$\boldsymbol{\varphi}^* = \arg \min_{\boldsymbol{\varphi} \in \Phi} \left[\frac{1}{N} \sum_{i=1}^N k(\boldsymbol{\varphi} | \boldsymbol{\theta}^j) \frac{p(\boldsymbol{\theta}^j)}{q(\boldsymbol{\theta}^j)} \right] \quad (31)$$

using the previously converged to optimum (stage 1) as an initial point (facilitating higher convergence efficiency for the second stage) and adopting an exterior sampling approach [46] and a sufficiently large N to reach high accuracy estimates (small coefficient of variation). The exterior sampling utilizes the same stream of common random numbers for all design configurations considered within the optimization described by Eq. (31); this creates a consistent estimation error and has significant computational benefits for the numerical optimization.

5. ILLUSTRATIVE APPLICATION

In this section the herein proposed optimum TMDI design approach is illustrated by considering a 10-storey building frame as the primary structure. Results for the *nominal design* (no uncertainties in the model description) and the *robust design* are separately discussed. The presentation starts with an overview of the structural and excitation models.

5.1 Structural and excitation models

A 10-storey lumped mass planar linear shear frame building is adopted as the primary structure with uncertain classical modal damping and uncertain floor stiffnesses being correlated between different floors. The lumped mass per story is 900ton whereas the nominal stiffness has a gradual decrease along height; it is 782.22MN/m for the bottom four stories, 626.10MN/m for the three intermediate ones and 469.57MN/m for the top three stories. The inter-story stiffness k_i of all the stories are parameterized by $k_i = \theta_{ki} \tilde{k}_i$, $i=1, \dots, n$, where \tilde{k}_i are the nominal values (mentioned above) and θ_{ki} are non-dimensional uncertain parameters, assumed to be correlated Gaussian variables with mean value one and covariance matrix with elements $\Sigma_{ik} = (0.1)^2 \exp[-(i-k)^2/2^2]$. This assumption implies significant correlation between inter-story stiffnesses within two stories apart and a coefficient of variation (c.o.v) of 10%. Modal damping is assumed for calculating the damping matrix $\mathbf{D}_s(\boldsymbol{\theta}_s)$ for the structure [47], with the damping ratio for all modes ζ taken to be a lognormally distributed random variable with median value equal to 0.035% and c.o.v 40%.

The stationary seismic excitation \ddot{x}_g is described by a high-pass filtered Kanai-Tajimi power spectrum [47]

$$S_g(\omega) = s_o \frac{\omega_g^4 + 4\zeta_g^2 \omega^2 \omega_g^2}{(\omega_g^2 - \omega^2)^2 + 4\zeta_g^2 \omega_g^2 \omega^2} \frac{\omega^4}{(\omega_f^2 - \omega^2)^2 + 4\zeta_f^2 \omega_f^2 \omega^2} \quad (32)$$

In the above equation the Kanai-Tajimi parameters ω_g and ζ_g represent the stiffness/frequency and damping properties, respectively, of the supporting ground modeled by a linear damped SDOF oscillator driven by white noise. Further, the parameters ω_f and ζ_f control the cut-off frequency and the “steepness” of a high-pass filter used to suppress the low frequency content allowed by the Kanai-Tajimi filter. Lastly, s_o is chosen to achieve a desired pre-specified value for the root mean square acceleration a_{RMS} of the considered seismic input. The state-space representation of this excitation model is given in Appendix A. For the purposes of this study, ω_g , ω_f , ζ_g , ζ_f and a_{RMS} are modeled as lognormal variables with median values 3π , $\pi/2$, 0.4 and 0.8, respectively, and coefficient of variation 15% for the frequency parameters, 30% for the damping parameters and 5% for a_{RMS} . The duration of excitation T is taken as 15 s. These choices lead to a 5-dimensional $\theta_q = [\omega_g \ \omega_f \ \zeta_g \ \zeta_f \ a_{RMS}]$ and a 11 dimensional $\theta_s = [\{\theta_{si}; i=1, \dots, 10\} \ \zeta]$.

The vector of structural performance variables $\mathbf{z}(t)$ includes inter-storey drifts, associated with the structural integrity of the primary structure, and absolute floor accelerations, associated with the response of secondary equipment (building contents) housed by the primary structure, for all 10 floors, as well as the TMD mass displacement, associated with the stroke of the damper and inerter and with the required clearance between the mass and the host structure ($n_z = 21$ performance variables in total). Note that the inerter force that needs to be transferred to the primary structure may also be of concern in practical implementations (i.e. might require some local strengthening of the structural frame to accommodate the inerter force). However, this force is not included in the performance variable vector as deformation and/or acceleration-based engineering demand parameters are usually monitored in the relevant literature [19, 27, 29, 32]. The assumed thresholds β_i are chosen as 3.3 cm for inter-storey drifts, 0.5g for floor accelerations, and 1m for the stroke (common for mass damper applications). For the structural performance variables the thresholds are chosen based on common fragility function recommendations [48]: the drift threshold is chosen to correspond to an intermediate failure mode (between moderate and severe damage) for partitions assuming a story-height of 4 m, and the acceleration threshold is chosen to correspond to damage to ceiling tiles. Without loss of generality, equal weights $w_i = 1/n_z$ are considered for all performance variables. This assumes equal consequences for all failure modes and was chosen (see discussion in next paragraph) to provide a comparable contribution to the total failure probability from the drift and acceleration related failure modes.

For the primary (uncontrolled) nominal structure (with median values for the structural properties), the objective function (average failure probabilities) is 12.38%. When considering only drift or acceleration responses this value becomes 10.94% or 13.83%, respectively. When uncertainty is considered only for the excitation model, these probabilities are 13.98% (total), 13.04% (drifts) and 14.91% (accelerations), respectively, whereas when uncertainty is additionally considered for the structural properties the probabilities increase to 17.56% (total), 17.43% (drifts) and 17.69% (accelerations), respectively.

The vector of dimensionless TMDI design variables, $\boldsymbol{\phi}$, includes the damping, frequency and inertance ratios, defined in Eq. (3), i.e., $\boldsymbol{\phi}=[\zeta_d f_d \beta]^T$. For the frequency ratio the nominal structural model characteristics are utilized in computing ω_1 . The mass ratio μ is treated as a fixed pre-specified variable and a parametric investigation is undertaken for different values of μ [given by Eq. (3)] ranging from 0.1% to 10% of the total structural mass. Since all 10 floors have equal mass, these values correspond, respectively, from 1% to 100% of the mass of the i_d floor where the TMD is attached to. The consideration of certain large attached mass cases (added mass up to the mass of a whole floor) is deemed to be useful to enable comparisons with large-mass TMDs for the seismic protection of building structures as suggested in the recent literature [13-17]. Nevertheless, as it will become clear in the numerical results, practical TMDI implementations should consider relatively small attached mass (small values of μ) for which the inclusion of the inerter is much more beneficial (see also [19]). In addition, the limiting case of the TID ($\mu=0$) [29] is also considered in the parametric investigation. For all pre-specified mass values examined, a set of 12 different TMDI topologies are assessed defined by i_d and i_b floor pairs (i.e., floor numbers where the TMD and the inerter are attached to, respectively). Note that, although practical architectural considerations suggest that the inerter would link the attached mass to the floor immediately above or below the i_d floor, cases in which $|i_d-i_b|=2$ are also examined here. Such topologies may be implemented, for example, by considering sufficiently large slab openings which may also be used in pendulum-like TMD applications (e.g., Taipei 101 building, Taiwan). TMDI topologies where the inerter spans more than two floors, i.e. $|i_d-i_b|>2$ are pertinent to tall buildings (e.g., [49]) and are considered as impractical for a 10-storey primary structure. They are not pursued here. Finally, the placement of the TMDI in the ground floor, $i_d=1$, is also examined, since it was recommended in [29] as the most effective TID location. It is, however, emphasized that placement towards the top floor of buildings is envisioned for the TMDI (as in the case of TMDs) to accommodate practical architectural considerations.

5.2 Optimum nominal design for deterministic excitation and structural model parameters

The proposed optimum TMDI design framework is first applied to a case that the model parameters of the adopted structure and excitation are deterministically known and set to their nominal (median) values to obtain *nominal designs*, $\boldsymbol{\phi}_n^*$, in Eq.(21). The optimum design problem for the $J(\boldsymbol{\phi}|\boldsymbol{\theta})$ in Eq.(22) is solved utilizing a standard nonlinear global optimization algorithm through the versatile TOMLAB optimization environment [50]. Optimal design for a TMD located at the top floor (i.e., the most widely-used in practice TMD location) are also obtained, by setting $\beta=0$ in the proposed design framework, to compare with the TMDI designs.

Moreover, a simplified optimum design denoted by $\boldsymbol{\phi}_s^*$ is also examined considering the minimization of the transfer function for the top floor response acceleration. That is,

$$\boldsymbol{\phi}_s^* = \arg \min_{\boldsymbol{\phi} \in \Phi} \left[\max_{\omega \in \mathbb{R}^+} |H_{z_i}(\omega|\boldsymbol{\phi}, \boldsymbol{\theta})| \right] \quad (33)$$

where the transfer function is given by Eq. (10) for z_i being the top floor acceleration. Adopting the sequence of the performance variables as discussed in the Appendix, the simplified design considers only the 20th element of the performance variables vector \mathbf{z} and is accomplished within the proposed design framework by populating the \mathbf{n}_i vector in Eq.(8) with zeros except for its 20th component set equal to 1. This simplified design considers the influence of the TMDI and TID

only close to the dominant structural mode and is ultimately similar to the classical optimization considered for TMDs, targeting only the fundamental mode of vibration. However, note that even this simplified design accounts, to some extent, for the higher-order dynamics through the floor acceleration sensitivity to high frequency response as shown in Figure 1(b).

The performance of the nominal design $J(\boldsymbol{\phi}_n^* | \boldsymbol{\theta})$ is shown in Table I for all the TMDI topologies and mass ratios considered, as well as for the top floor TMD. The inertance ratio β under optimal design is also reported. Due to space constraints, the rest of the optimal TMDI parameters are not reported here, as they are deemed less important and, in general, follow the same trends presented elsewhere in the literature [18, 19]. Note that optimal TMDI configurations leading to a TMD (i.e., optimal inertance value $\beta=0$) are explicitly denoted with a superscript ⁺ in Table I. This consideration further highlights the practical usefulness of interpreting the TMDI as a generalization of the TMD [20] and establishes the potential of the proposed framework to serve as a unified optimum design platform for TMDs, TMDIs and TIDs.

During optimization, it is found that a manifold of near-optimal solutions, i.e. values of $\boldsymbol{\phi}$ that yield almost the same performance, exist in all cases considered. This is attributed to the fact that the objective function is a combination of different failure modes and so design configurations that yield a different balance between these modes result in a similar overall performance. In this regard, the focus of the discussion herein is on the optimal performance rather than on the corresponding optimal configurations. In this regard, the reported numerical data in Table I suggests that a definite optimum inertance ratio β exists, whose value depends on the mass ratio μ as well as on the TMDI topology. Above a certain critical mass ratio value, the classical TMD (no inerter included) achieves better performance. This trend indicates that the mass amplification effect of the inerter saturates as higher mass values are considered and that there are bounds to the extent that the inertance property can effectively substitute the mass property. More importantly from a practical viewpoint, it is evident that *the inclusion of the inerter device is more beneficial for relatively small attached masses*: an observation previously reported in the literature in terms of top floor displacement variance minimization [19]. Herein, it is further found that the lower the floor the TMDI mass is placed, the higher the mass ratio needed for the TMD to outperform the TMDI. This is readily explained by the fact that the efficiency of the TMD (i.e., its capability to suppress vibrations for the same attached mass) becomes higher as it is installed in higher floors of buildings with smooth floor stiffness and mass distribution in elevation as the one under consideration.

Turning the attention to the dependency of the TMDI performance on different topologies, it is seen that better performance is achieved for $i_d > i_b$ compared to the $i_d < i_b$, i.e. the attached mass is linked to a lower rather than an upper floor via the inerter (this is the reason why for $i_d=7$ only cases with smaller i_b are reported). Moreover, *significantly improved performance is achieved for $|i_d - i_b|=2$ compared to $|i_d - i_b|=1$ topologies, i.e., by letting the inerter span more than one story*. The latter result is explained by inspecting the FRFs in Figures 1(b) or in Figure 2 (discussed later) where it is seen that optimal TMDI designs with $i_d - i_b = 2$ are more effective in reducing the FRF ordinates across all frequencies than $i_d - i_b = 1$. This may be intuitively attributed to the better inerter engagement achieved by the $|i_d - i_b|=2$ topologies as the inerter terminals are less likely to observe in-phase accelerations. This is because the inerter couples more “distant” DOFs in the controlled structure which are potentially less correlated. As a final remark, it is noted that the TID placed at

the ground floor does perform extraordinarily well, but not better than certain TMDIs with $|i_d - i_b| = 2$ topologies.

Results for the simplified design, which considers a single performance variable, are discussed next. Table II reports the ratio $J(\boldsymbol{\varphi}_s^* | \boldsymbol{\theta}) / J(\boldsymbol{\varphi}_n^* | \boldsymbol{\theta})$ to quantify the performance degradation if $\boldsymbol{\varphi}_s^*$ design is considered instead of $\boldsymbol{\varphi}_n^*$ (larger values correspond to larger performance degradation). The optimal inertance ratio for $\boldsymbol{\varphi}_s^*$ is also reported in Table II. TMDI topologies with $i_d < i_b$ are dropped from Table II since are not recommended based on the results in Table I.

Notably, the performance degradation for the TMD configurations is relatively low, which confirms that aiming to suppress response oscillations related to a single (the fundamental) mode by optimizing for the most relevant DOF (in this case top floor DOF where the modal ordinate of the fundamental mode shape peaks) yields a TMD configuration compatible with other design approaches. Still, accounting for more than one DOF in the objective function $J(\boldsymbol{\varphi} | \boldsymbol{\theta})$ as considered in the proposed optimum design approach may yield better performance even for the TMD. As anticipated, significant performance degradation between the nominal and the simplified design is observed for the TMDI demonstrating that its optimal design is sensitive to the performance variables considered. Indeed, the two optimum design points differ significantly as evidenced by the differences to the optimal inertance ratio values between Tables I and II. To shed light in this behavior, Figure 2 plots the absolute top floor acceleration FRFs for $\boldsymbol{\varphi}_s^*$ and $\boldsymbol{\varphi}_n^*$ for three different configurations, one corresponding to TMD and two to TMDI (the behavior of the TID is similar as mass ratio has a minor only influence). Evidently, the nominal TMDI design achieves significant reduction to the plotted FRFs along the whole frequency axis compared to the simplified design (similar trends are observed for all other topologies examined). This observation confirms the point discussed in the introduction: efficient optimum TMDI design requires adopting performance variables that facilitates the TMDI higher-mode-damping effect to the primary structure over a broad frequency range, and not only close to the fundamental structural frequency. Clearly, the proposed optimum TMDI approach fulfils this objective.

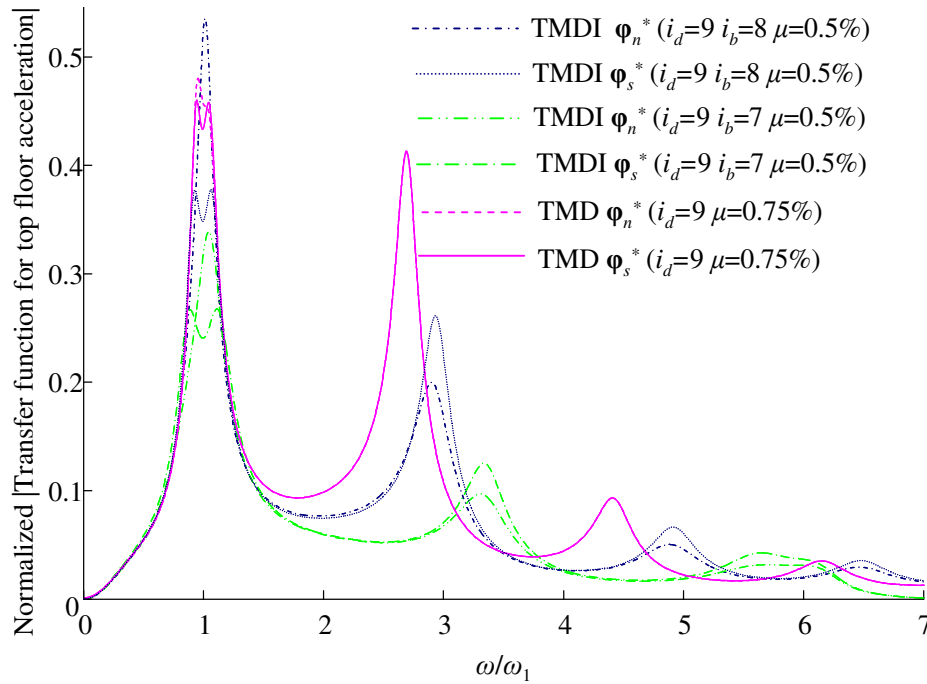


Figure 2: Normalized absolute FRFs for top floor acceleration for nominal, ϕ_n^* , and simplified, ϕ_s^* , designs for two different TMDIs and one TMD. Normalization is with respect to the peak value of the uncontrolled structure.

5.3 Optimum robust design for uncertain excitation and structural model parameters

The applicability of the proposed design framework to treat model uncertainty is illustrated by examining two different *robust design* cases, ϕ^* , in Eq. (30): the first, termed *robust-exc*, considers uncertainty only to the seismic excitation properties, while the second, termed *robust-full*, considers uncertainty to both the excitation and the structural model. In both design cases, the probabilistic integral in Eq.(26) is transformed to the standard Gaussian space and the two-stage approach discussed in section 4.2.2 is adopted for the numerical optimization. For the second stage, $N=5000$ samples are used for the stochastic simulation which yield a sufficiently low c.o.v, less than 2% for most design configurations examined. The proposal densities in the second stage are taken as independent Gaussian distributions for each uncertain model parameter with standard deviation equal to 1 and mean the design point θ^* identified in the first stage.

The optimal performance $J(\phi^*)$ and the inertance under optimal design are reported in Tables III and IV for the *robust-exc* and the *robust-full* cases, respectively. The same trends observed for the nominal design hold for the robust design as well, in terms of both TMDI effectiveness for different topologies and attached mass values vis-à-vis the TMD and the TID. Further, by comparing the numerical values in Tables III and IV to the corresponding ones in Table I, it is seen that parametric model uncertainty deteriorates the performance under optimal design. Uncertainty to the structural model has a more detrimental influence to performance deterioration than uncertainty to only the excitation, while more significant performance deterioration is observed for TMDI topologies that perform better under the nominal design, $J(\phi^* | \theta)$ (i.e. the lower the value of $J(\phi^* | \theta)$, the higher the difference $J(\phi^*) - J(\phi^* | \theta)$ is). These trends should be attributed to the fact that an increase of the uncertainty, i.e. including first uncertainty to the excitation model

only and, then, further increasing the number of uncertain parameters by introducing uncertainty to the structural model as well, has higher likelihood for impacting the performance for TMDI topologies achieving high performance for no uncertainty, that is, for structural response quantities that remain largely below the acceptable thresholds under stationary excitation [37].

Moreover, the impact of the uncertainty is greater for the performance of the TMDI than for the TMD. This can be seen by comparing the $J(\boldsymbol{\varphi}^*)$ values for different TMD and TMDI configurations that have similar $J(\boldsymbol{\varphi}^*|\boldsymbol{\theta})$ values. This trend is justified by considering that the TMDI impacts the structural performance over a much broader frequency range than the TMD. Therefore, the TMD performance is affected only to the extent that the uncertainty to model parameters influences the narrow frequency range that the TMD operates upon, while the influence of the same level of uncertainty to the TMDI performance is more significant as it impacts the broader frequency range which the TMDI “sees” (or operates upon). Consequently, for TMD applications, the design needs to ultimately consider only the uncertainties that impact the fundamental mode of the structure. However, TMDI design needs to take into account uncertainties that impact higher modes as well; a requirement that is well met by the proposed design framework as seen by the reported results and their interpretation.

Nevertheless, the fact that the performance deterioration under the nominal and the robust design is higher for the TMDI vis-à-vis the TMD must not be interpreted as higher robustness for the TMD. To quantify robustness to uncertainty, the ratio $J(\boldsymbol{\varphi}_n^*)/J(\boldsymbol{\varphi}^*)$ is reported in Table V, representing the ratio of performance of the nominal (deterministic) design under excitation and structural model uncertainty to the *robust-full* design performance (i.e., design accounting for uncertainty). These ratios clearly indicate that the TMDI enjoys a very high degree of robustness with respect to structural and excitation uncertainties: the performance $J(\boldsymbol{\varphi}_n^*)$ is very similar to $J(\boldsymbol{\varphi}^*)$ for all TMDI topologies examined. However, this is not the case for the TMD especially when its impact to the structural response is high (large mass ratios), for which differences exist between these two performances. These differences relate to detuning of the TMD as they appear when uncertainty in the structural model is introduced: the ratio $J(\boldsymbol{\varphi}_n^*)/J(\boldsymbol{\varphi}^*)$ for the *robust-exc* case (uncertainty only to the excitation) is close to one for both the TMDI and the TMD. Overall these comparisons indicate that TMDI design is not significantly influenced by the different sources of uncertainty, whereas the TMD design is impacted by uncertainties in the structural model. It must be emphasized, however, that the large differences $J(\boldsymbol{\varphi}^*) - J(\boldsymbol{\varphi}^*|\boldsymbol{\theta})$ in Tables I, III, and IV suggest that uncertainties may be ignored in deriving the optimal TMDI design solution, but should be considered for TMDI performance assessment.

6. CONCLUDING REMARKS

A design framework for seismically excited TMDI-equipped multi-storey buildings was established. The seismic excitation was modeled as stationary colored random process and the primary/host structure as a linear damped MDOF structural system. The considered framework accounts for the mass amplification and higher-modes-damping effects endowed by the inerter to the considered structural system while treats the TMD and the TID as special cases. In particular, the mass amplification effect is accounted for in the design by taking the inertance as a design parameter, along with the TMDI stiffness and damping properties. Further, the higher-modes-damping effect is taken into consideration in the optimization/design problem in a three-fold

manner: (i) by considering floor accelerations, apart from inter-storey drifts and attached mass displacement, as structural performance variables being sensitive to high-frequency structural response dynamics and, therefore, to higher modes, (ii) by expressing the structural performance (i.e., design objective function to be minimized) as a linear combination of the first-passage reliability of the above performance variables (i.e., probabilities that the monitored response quantities remain below given thresholds) whose quantification requires the consideration of the overall (broadband) structural response along the whole frequency axis and not around some specific frequency range/mode, and (iii) by adopting a state-space formulation to compute the structural response statistics involved in the calculation of the aforementioned reliabilities utilizing the initial equations of motion without taking any modal truncation step. The three considerations listed above ensure that the contribution from all structural modes to the evaluation of the design objective function is explicitly accounted for, leading to optimal designs across the full frequency range.

Moreover, the adopted framework accounts for, if deemed desirable, the uncertainty stemming from both the seismic excitation and the structural model in the TMDI design. This is achieved by letting any of the underlying excitation and/or structural model parameters be random variables. In this regard, two different design scenarios with respect to the nature of uncertainty accounted for in design were presented. The first (nominal design) scenario assumes that all model parameters are deterministically known and, therefore, uncertainty stems only from the stochastic characterization of the excitation. The second (robust design) scenario incorporates additionally parametric uncertainties to the excitation model (“robust-exc”) and to both the excitation and structural model (“robust-full”). In the first design scenario, structural performance is analytically quantified through the conditional out-crossing rate. Standard numerical optimization tools were then employed for performing the design optimization. In the second design scenario, the performance is expressed by a probabilistic integral, obtained by using the total probability theorem, and both analytic and stochastic-simulation tools were discussed for its calculation, adopting ultimately an efficient two-stage optimization scheme.

The proposed framework was applied to a 10-storey building frame under stationary high-pass filtered Kanai-Tajimi stochastic excitation. Numerical results pertaining to the optimal TMDI design for 12 different TMDI topologies and 13 secondary/attached mass values including the special case of zero attached mass (TID), with and without parametric uncertainty to the building and excitation models were furnished. In view of this data, attention was focused on highlighting: (I) the differences of the achieved structural performance between the herein reliability-based design framework accounting for higher-modes-damping effect and evaluating performance within a wide range of frequencies vis-a-vis a simplified design approach (often applied in TMD optimum design) focusing on controlling a single (the fundamental) mode and evaluating performance within a narrow frequency range around the first (fundamental) structural natural frequency, (II) the importance of the topological configuration for the TMDI to the achieved structural performance and required inertance ratio, and (III) the impact of parametric uncertainty (i.e. difference between nominal and robust design scenarios). Regarding point (I), it was found that considerably more effective TMDI design (but not TMD) is achieved through the adoption of the herein developed optimization framework confirming its capability to capture the higher-order dynamics and the influence of the TMDI in damping all (higher-) modes. Moreover, it was found

that the inclusion of the inerter accomplishes enhanced performance improvement compared to same-mass TMDs for smaller TMD mass and for TMDI topologies where the inerter links the TMD mass to two floors below the floor that the TMD is attached to. The placement of the attached mass to lower floors (but not necessarily to the ground floor) enables further performance improvement. These topologies yield significantly reduced frequency response function ordinates across the whole frequency domain. Lastly, parametric uncertainty to the excitation was shown to have a minor only impact for TMDs and TMDIs (including TIDs), whereas structural uncertainty was demonstrated to have a noticeable impact on the former and a negligible impact on the latter. This shows that the TMDI enjoys considerable robustness attributes and that the excitation characteristics have limited impact on the actual optimal design. Still, uncertainty to excitation and structural model have considerable impact on the achieved performance and should be appropriately accounted for in assessing that performance.

Overall, the reported numerical data validate previous results and trends and shed new light on the potential of the TMDI as a seismic protection system. Nevertheless, a detailed life-cycle assessment of the economic benefits of the TMDI vis-à-vis the TMD and/or other passive vibration control solutions for the task remain a topic of future work for the authors. To this aim, several practical aspects needs to be accounted for such as the deviation of the inerter from the linear behavior, the uncertainty to the TMDI properties, the potentially non-linear structural response, and the additional cost of accommodating the potentially large inerter forces transmitted to the host/primary structure associated with special local connection detailing.

APPENDIX A: STATE SPACE FORMULATION

The state-space representation of the TMDI-equipped n -story structure in Eqs. (1) and (2) reads

$$\begin{aligned}\dot{\mathbf{x}}_{ss}(t) &= \mathbf{A}_s(\boldsymbol{\varphi}, \boldsymbol{\theta}_s) \mathbf{x}_{ss}(t) + \mathbf{E}_s(\boldsymbol{\varphi}, \boldsymbol{\theta}_s) \ddot{\mathbf{x}}_g(t) \\ \mathbf{z}(t) &= \mathbf{C}_s(\boldsymbol{\varphi}, \boldsymbol{\theta}_s) \mathbf{x}_{ss}(t)\end{aligned}\tag{34}$$

where $\mathbf{x}_{ss} \in \mathbb{R}^{2n+2}$ is the state vector collecting relative to the ground displacements and velocities of all stories and of the attached mass (relative to i_b floor), $\mathbf{x}_s = [\mathbf{x}_s^T \quad y \quad \dot{\mathbf{x}}_s^T \quad \dot{y}]^T$, and the matrices in Eq. (34) are defined as

$$\begin{aligned}
 \mathbf{A}_s(\boldsymbol{\varphi}, \boldsymbol{\theta}_s) &= \begin{bmatrix} \mathbf{0}_{(n+1) \times (n+1)} & \mathbf{I}_{(n+1)} \\ -\mathbf{M}_t^{-1}(\boldsymbol{\varphi}, \boldsymbol{\theta}_s) \begin{bmatrix} \mathbf{K}_s(\boldsymbol{\theta}_s) & \mathbf{0}_{n \times 1} \\ \mathbf{0}_{1 \times n} & k_d \end{bmatrix} & -\mathbf{M}_t^{-1}(\boldsymbol{\varphi}, \boldsymbol{\theta}_s) \begin{bmatrix} \mathbf{C}_s(\boldsymbol{\theta}_s) & \mathbf{0}_{n \times 1} \\ \mathbf{0}_{1 \times n} & c_d \end{bmatrix} \end{bmatrix} \\
 \mathbf{E}_s(\boldsymbol{\varphi}, \boldsymbol{\theta}_s) &= \begin{bmatrix} \mathbf{0}_{(n+1) \times 1} \\ -\mathbf{M}_t^{-1}(\boldsymbol{\varphi}, \boldsymbol{\theta}_s) \begin{bmatrix} \mathbf{M}_s(\boldsymbol{\theta}_s) + \mathbf{R}_d m_d \mathbf{R}_d^T \\ m_d \mathbf{R}_d^T \end{bmatrix} \mathbf{R}_s \end{bmatrix} \\
 \mathbf{C}_s(\boldsymbol{\varphi}, \boldsymbol{\theta}_s) &= \begin{bmatrix} \mathbf{T}_s & \mathbf{0}_{n \times (n+2)} \\ -\begin{bmatrix} \mathbf{I}_n & \mathbf{0}_{(n+1) \times 1} \end{bmatrix} \mathbf{M}_t^{-1}(\boldsymbol{\varphi}, \boldsymbol{\theta}_s) \begin{bmatrix} \mathbf{K}_s(\boldsymbol{\theta}_s) & \mathbf{0}_{n \times 1} \\ \mathbf{0}_{1 \times n} & k_d \end{bmatrix} \begin{bmatrix} \mathbf{C}_s(\boldsymbol{\theta}_s) & \mathbf{0}_{n \times 1} \\ \mathbf{0}_{1 \times n} & c_d \end{bmatrix} \\ \mathbf{0}_{1 \times n} & 1 & \mathbf{0}_{1 \times (n+1)} \end{bmatrix}
 \end{aligned} \tag{35}$$

In the above expressions, the output matrix $\mathbf{C}_s(\boldsymbol{\varphi}, \boldsymbol{\theta}_s)$ accounts for a performance (output) variables vector \mathbf{z} that includes inter-storey drifts and absolute accelerations for all floors, as well as the attached mass displacement as considered in the illustrative design example, \mathbf{I}_a is the identity matrix of dimension a , $\mathbf{0}_{a \times b}$ is the zero matrix of dimensions $a \times b$, \mathbf{T}_s is a transformation matrix defining relative responses between consecutive floors (i.e., a square matrix with dimension n_s with 1 in the diagonal and -1 in the first off-diagonal), and the auxiliary matrix \mathbf{M}_t reads as

$$\mathbf{M}_t(\boldsymbol{\varphi}, \boldsymbol{\theta}_s) = \begin{bmatrix} \mathbf{M}_s(\boldsymbol{\theta}_s) + \mathbf{R}_d m_d \mathbf{R}_d^T + \mathbf{R}_c b \mathbf{R}_c^T & m_d \mathbf{R}_d + b \mathbf{R}_c \\ m_d \mathbf{R}_d^T + b \mathbf{R}_c^T & m_d + b \end{bmatrix}. \tag{36}$$

Combining Eqs. (34) and (4) leads to the representation in Eq. (5) where

$$\begin{aligned}
 \mathbf{x} &= \begin{bmatrix} \mathbf{x}_{ss} \\ \mathbf{x}_f \end{bmatrix} & \mathbf{A}(\boldsymbol{\varphi}, \boldsymbol{\theta}) &= \begin{bmatrix} \mathbf{A}_s(\boldsymbol{\varphi}, \boldsymbol{\theta}_s) & \mathbf{E}_s(\boldsymbol{\varphi}, \boldsymbol{\theta}_s) \mathbf{C}_q(\boldsymbol{\theta}_q) \\ \mathbf{0}_{n_q \times (2n+2)} & \mathbf{A}_q(\boldsymbol{\varphi}, \boldsymbol{\theta}_q) \end{bmatrix} \\
 \mathbf{E} &= \begin{bmatrix} \mathbf{0}_{2(n+1) \times 1} \\ \mathbf{E}_q \end{bmatrix} & \mathbf{C}(\boldsymbol{\varphi}, \boldsymbol{\theta}) &= \begin{bmatrix} \mathbf{C}_s(\boldsymbol{\varphi}, \boldsymbol{\theta}) & \mathbf{0}_{n_z \times n_q} \end{bmatrix}
 \end{aligned} \tag{37}$$

Lastly, the state-space matrices of the excitation model assumed in the design example read as

$$\begin{aligned}
 \mathbf{A}_q &= \begin{bmatrix} 0 & 1 & 0 & 0 \\ -\omega_g^2 & -2\zeta_g \omega_g & 0 & 0 \\ 0 & 0 & 0 & 1 \\ -\omega_f^2 & -2\zeta_g \omega_g & -\omega_f^2 & -2\zeta_f \omega_f \end{bmatrix} & \mathbf{E}_q &= \begin{bmatrix} 0 \\ 1 \\ 0 \\ 0 \end{bmatrix} \\
 \mathbf{C}_q &= \sigma_o \begin{bmatrix} -\omega_g^2 & -2\zeta_g \omega_g & \omega_f^2 & 2\zeta_f \omega_f \end{bmatrix}
 \end{aligned} \tag{38}$$

where σ_o is chosen such that the excitation has the desired RMS intensity.

ACKNOWLEDGEMENTS

The first author gratefully acknowledges the financial support by EPSRC in UK, under grant EP/M017621/1.

REFERENCES

1. Den Hartog, J.P., *Mechanical Vibrations*. 1947, New York, NY: McGraw-Hill, Inc.
2. Kareem, A. and S. Kline, Performance of multiple mass dampers under random loading. *Journal of Structural engineering, ASCE*, 1993. **121**(2): p. 348-361.
3. Soto, M.G. and H. Adeli, Tuned mass dampers. *Archives of Computational Methods in Engineering*, 2013. **20**(4): p. 419-431.
4. Chang, C.C., Mass dampers and their optimal designs for building vibration control *Engineering Structures*, 1999. **21**: p. 454-463.
5. Kareem, A., T. Kijewski, and Y. Tamura, Mitigation of motions of tall buildings with specific examples of recent applications. *Wind and structures*, 1999. **2**(3): p. 201-251.
6. Rana, R. and T.T. Soong, Parametric study and simplified design of tuned mass dampers. *Engineering Structures*, 1998. **20**(3): p. 193-204.
7. Tigli, O.F., Optimum vibration absorber (tuned mass damper) design for linear damped systems subjected to random loads. *Journal of sound and vibration*, 2012. **331**(13): p. 3035-3049.
8. Chakraborty, S. and B.K. Roy, Reliability based optimum design of tuned mass damper in seismic vibration control of structures with bounded uncertain parameters. *Probabilistic Engineering Mechanics*, 2011. **26**(2): p. 215-221.
9. Marano, G.C., R. Greco, F. Trentadue, and B. Chiaia, Constrained reliability-based optimization of linear tuned mass dampers for seismic control. *International Journal of Solids and Structures*, 2007. **44**(22-23): p. 7370-7388.
10. Taflanidis, A.A., J.L. Beck, and D.A. Angelides, Robust reliability-based design of liquid column mass dampers under earthquake excitation using an analytical reliability approximation. *Engineering Structures*, 2007. **29**(12): p. 3525-3537.
11. Singh, M.P., S. Singh, and L.M. Moreschi, Tuned mass dampers for response control of torsional buildings. *Earthquake Engineering and Structural Dynamics*, 2002. **31**: p. 749-769.
12. De Angelis, M., S. Perno, and A. Reggio, Dynamic response and optimal design of structures with large mass ratio TMD. *Earthquake Engineering & Structural Dynamics*, 2012. **41**(1): p. 41-60.
13. Hoang, N., Y. Fujino, and P. Warnitchai, Optimal tuned mass damper for seismic applications and practical design formulas. *Engineering Structures*, 2008. **30**(3): p. 707-715.
14. Matta, E., Performance of tuned mass dampers against near-field earthquakes. *Structural Engineering and Mechanics*, 2011. **39**(5): p. 621-642.
15. Matta, E. and A. De Stefano, Seismic performance of pendulum and translational roof-garden TMDs. *Mechanical Systems and Signal Processing*, 2009. **23**(3): p. 908-921.
16. Moutinho, C., An alternative methodology for designing tuned mass dampers to reduce seismic vibrations in building structures. *Earthquake Engineering & Structural Dynamics*, 2012. **41**(14): p. 2059-2073.
17. Tian, Z., J. Qian, and L. Zhang, Slide roof system for dynamic response reduction. *Earthquake Engineering & Structural Dynamics*, 2008. **37**(4): p. 647-658.
18. Marian, L. and A. Giaralis. Optimal design of inerter devices combined with TMDs for vibration control of buildings exposed to stochastic seismic excitations. in *11th International Conference on Structural Safety and Reliability*. 2013. New York, US.
19. Marian, L. and A. Giaralis, Optimal design of a novel tuned mass-damper-inerter (TMDI) passive vibration control configuration for stochastically support-excited structural systems. *Probabilistic Engineering Mechanics*, 2014. **38**: p. 156-164.
20. Smith, M.C., Synthesis of mechanical networks: the inerter. *Automatic Control, IEEE Transactions on*, 2002. **47**(10): p. 1648-1662.

Giaralis A, Taflanidis AA. Optimal tuned mass-damper-inerter (TMDI) design for seismically excited MDOF structures with model uncertainties based on reliability criteria. *Struct Control Health Monit.* 2017;e2082. <https://doi.org/10.1002/stc.2082>

21. Papageorgiou, C. and M.C. Smith. *Laboratory experimental testing of inerters.* in *Decision and Control, 2005 and 2005 European Control Conference. CDC-ECC'05. 44th IEEE Conference on.* 2005: IEEE.
22. Wang, F.-C., M.-F. Hong, and T.-C. Lin, Designing and testing a hydraulic inerter. *Proceedings of the Institution of Mechanical Engineers, Part C: Journal of Mechanical Engineering Science*, 2011. **225**(1): p. 66-72.
23. Swift, S.J., M.C. Smith, A.R. Glover, C. Papageorgiou, B. Gartner, and N.E. Houghton, Design and modelling of a fluid inerter. *International Journal of Control*, 2013. **86**(11): p. 2035-2051.
24. Gonzalez- Buelga, A., I.F. Lazar, J.Z. Jiang, S.A. Neild, and D.J. Inman, Assessing the effect of nonlinearities on the performance of a tuned inerter damper. *Structural Control and Health Monitoring*, 2016. **24**(3): p. e1879.
25. Takewaki, I., S. Murakami, S. Yoshitomi, and M. Tsuji, Fundamental mechanism of earthquake response reduction in building structures with inertial dampers. *Structural Control and Health Monitoring*, 2012. **19**(6): p. 590-608.
26. Hwang, J.-S., J. Kim, and Y.-M. Kim, Rotational inertia dampers with toggle bracing for vibration control of a building structure. *Engineering Structures*, 2007. **29**(6): p. 1201-1208.
27. Ikago, K., K. Saito, and N. Inoue, Seismic control of single-degree-of-freedom structure using tuned viscous mass damper. *Earthquake Engineering & Structural Dynamics*, 2012. **41**(3): p. 453-474.
28. Ikago, K., Y. Sugimura, K. Saito, and N. Inoue, Modal response characteristics of a multiple-degree-of-freedom structure incorporated with tuned viscous mass dampers. *Journal of Asian Architecture and Building Engineering*, 2012. **11**(2): p. 375-382.
29. Lazar, I.F., S.A. Neild, and D.J. Wagg, Using an inerter-based device for structural vibration suppression. *Earthquake Engineering & Structural Dynamics*, 2014. **43**(8): p. 1129-1147.
30. Marian, L. and A. Giaralis, The tuned mass-damper-inerter for harmonic vibrations suppression, attached mass reduction, and energy harvesting. *Smart Structures and Systems*, 2017(DOI:10.12989/sss.2017.19.6.000).
31. Zhang, S.Y., J.Z. Jiang, and S. Neild, Optimal configurations for a linear vibration suppression device in a multi- storey building. *Structural Control and Health Monitoring*, 2017. **24**(3): p. e1887.
32. Krenk, S. and J. Høgsberg, Tuned resonant mass or inerter-based absorbers: unified calibration with quasi-dynamic flexibility and inertia correction. *Proceedings of the Royal Socociety A*, 2016. **472**: p. 20150718.
33. Taflanidis, A.A. and J.T. Scruggs, Performance measures and optimal design of linear structural systems under stochastic stationary excitation. *Structural Safety*, 2010. **32**(5): p. 305-315.
34. Singh, M.P. and L.M. Moreschi, Optimal placement of dampers for passive response control. *Earthquake Engineering & Structural Dynamics*, 2002. **31**(4): p. 955-976.
35. Goulet, C.A., C.B. Haselton, J. Mitrani-Reiser, J.L. Beck, G. Deierlein, K.A. Porter, and J.P. Stewart, Evaluation of the seismic performance of code-conforming reinforced-concrete frame building-From seismic hazard to collapse safety and economic losses. *Earthquake Engineering and Structural Dynamics*, 2007. **36**(13): p. 1973-1997.
36. Lutes, L.D. and S. Sarkani, *Random vibrations : analysis of structural and mechanical systems.* 2004, Amsterdam ; Boston: Elsevier.
37. Taflanidis, A.A., J.T. Scruggs, and J.L. Beck, Reliability-based performance objectives and probabilistic robustness in structural control applications. *Journal of Engineering Mechanics*, 2008. **134**(4): p. 291-301.
38. Porter, K.A., A.S. Kiremidjian, and J.S. LeGrue, Assembly-based vulnerability of buildings and its use in performance evaluation. *Earthquake Spectra*, 2001. **18**(2): p. 291-312.
39. Taflanidis, A.A. and J.L. Beck, Analytical approximation for stationary reliability of certain and uncertain linear dynamic systems with higher dimensional output. *Earthquake Engineering and Structural Dynamics*, 2006. **35**(10): p. 1247-1267.

40. Rice, S.O., Mathematical analysis of random noise. *Bell System Technical Journal*, 1944, 1945. **23 and 24**.
41. Lutes, L.D. and S. Sarkani, *Stochastic analysis of structural and mechanical vibrations*. 1997, Upper Saddle River, NJ: Prentice Hall.
42. Papadimitriou, C., J. Beck, and L. Katafygiotis, Asymptotic expansions for reliabilities and moments of uncertain dynamic systems. *Journal of Engineering Mechanics*, 1997. **123**: p. 1219-1229.
43. Au, S.K., C. Papadimitriou, and J.L. Beck, Reliability of uncertain dynamical systems with multiple design points. *Structural Safety*, 1999. **21**: p. 113-133.
44. Taflanidis, A.A., Reliability-based optimal design of linear dynamical systems under stochastic stationary excitation and model uncertainty. *Engineering Structures*, 2010. **32**(5): p. 1446-1458.
45. Robert, C.P. and G. Casella, *Monte Carlo Statistical Methods*. 2nd ed. 2004, New York, NY: Springer.
46. Spall, J.C., *Introduction to stochastic search and optimization*. 2003, New York: Wiley-Interscience.
47. Clough, R.W. and J. Penzien, *Dynamics of structures*. 1993, New York, N.Y: McGraw-Hill Inc.
48. Gidaris, I. and A.A. Taflanidis, Performance assessment and optimization of fluid viscous dampers through life-cycle cost criteria and comparison to alternative design approaches. *Bulletin of Earthquake Engineering*, 2015. **13**(4): p. 1003-1028.
49. Giaralis, A. and F. Petrini, Wind-induced vibration mitigation in tall buildings using the tuned mass-damper-inerter (TMDI). *Journal of Structural Engineering, ASCE*, 2017. **accepted**.
50. Holmstrom, K., A.O. Goran, and M.M. Edvall, *User's guide for TOMLAB 7*. 2009, San Diego, CA: Tomlab Optimization Inc. www.tomopt.com/tomlab/.

Table I: Optimal performance under nominal design $J(\Phi_n^* | \Theta)$ [%] and optimal inertance ratios β (%) in parenthesis.

TMDI with topologies defined through i_d, i_b														
i_d	i_b	Mass ratio μ (%)												
		TID ($\mu=0$)	0.1	0.3	0.5	0.6	0.75	1	1.5	2	3	5	7	10
10	9	6.123 (199.9)	6.077 (198.6)	5.976 (195.4)	5.726 (192.4)	5.169 ⁺ (0.0)	4.438 ⁺ (0.0)	3.610 ⁺ (0.0)	2.688 ⁺ (0.0)	2.152 ⁺ (0.0)	1.454 ⁺ (0.0)	0.671 ⁺ (0.0)	0.299 ⁺ (0.0)	0.091 ⁺ (0.0)
10	8	1.052 (103.0)	1.036 (102.5)	1.002 (101.2)	0.969 (100.0)	0.952 (99.1)	0.929 (98.4)	0.890 (96.8)	0.818 (93.6)	0.751 (90.3)	0.633 (83.0)	0.440 (65.3)	0.284 (45.8)	0.091 ⁺ (0.0)
9	10	6.129 (200.4)	6.142 (202.7)	6.169 (206.8)	6.002 (202.5)	5.410 ⁺ (0.0)	4.683 ⁺ (0.0)	3.853 ⁺ (0.0)	2.937 ⁺ (0.0)	2.424 ⁺ (0.0)	1.783 ⁺ (0.0)	1.058 ⁺ (0.0)	0.637 ⁺ (0.0)	0.295 ⁺ (0.0)

9	8	1.923 (208.2)	1.909 (207.5)	1.880 (205.2)	1.852 (203.1)	1.838 (202.2)	1.817 (200.6)	1.783 (197.9)	1.718 (192.6)	1.657 (185.1)	1.541 (175.9)	1.058 ⁺ (0.0)	0.637 ⁺ (0.0)	0.295 ⁺ (0.0)
9	7	0.120 (134.3)	0.119 (133.4)	0.118 (133.0)	0.117 (129.3)	0.116 (128.6)	0.115 (127.0)	0.114 (125.4)	0.111 (121.7)	0.109 (121.0)	0.103 (111.1)	0.092 (92.6)	0.078 (72.6)	0.052 (46.6)
8	9	1.925 (208.8)	1.933 (210.4)	1.950 (215.2)	1.967 (219.1)	1.976 (221.2)	1.989 (222.1)	2.014 (233.1)	2.063 (311.7)	2.089 (316.5)	2.155 (324.1)	1.544 ⁺ (0.0)	1.184 ⁺ (0.0)	0.852 ⁺ (0.0)
8	10	1.054 (103.2)	1.060 (104.4)	1.070 (105.5)	1.082 (108.9)	1.088 (110.2)	1.097 (112.2)	1.118 (140.3)	1.129 (142.8)	1.144 (145.1)	1.187 (149.6)	1.323 (158.3)	1.184 ⁺ (0.0)	0.852 ⁺ (0.0)
8	7	0.914 (233.3)	0.911 (231.5)	0.903 (222.8)	0.896 (230.8)	0.892 (230.6)	0.886 (228.7)	0.877 (228.5)	0.860 (222.1)	0.843 (220.3)	0.812 (216.8)	0.753 (194.7)	0.700 (172.8)	0.615 (127.2)
8	6	0.093 (151.9)	0.093 (151.2)	0.092 (152.1)	0.091 (146.7)	0.091 (151.7)	0.091 (146.4)	0.090 (151.9)	0.088 (146.7)	0.087 (143.9)	0.086 (154.4)	0.080 (131.3)	0.077 (126.7)	0.071 (100.9)
7	6	1.026 (299.8)	1.022 (299.2)	1.014 (298.2)	1.006 (297.8)	1.003 (298.8)	0.997 (298.5)	0.987 (298.5)	0.968 (296.6)	0.949 (295.3)	0.912 (292.1)	0.844 (285.7)	0.783 (279.3)	0.707 (253.0)
7	5	0.067 (165.9)	0.066 (166.1)	0.065 (166.1)	0.064 (166.3)	0.064 (166.3)	0.063 (166.6)	0.062 (166.8)	0.059 (167.0)	0.057 (167.7)	0.052 (168.4)	0.045 (170.2)	0.039 (170.9)	0.033 (166.6)
1	0	0.277 (426.3)	0.277 (422.8)	0.276 (422.8)	0.276 (432.2)	0.275 (423.5)	0.275 (424.2)	0.274 (432.4)	0.273 (425.1)	0.271 (427.6)	0.269 (428.8)	0.264 (431.8)	0.259 (432.0)	0.252 (438.6)
TMD at top floor														
$i_d=10$	$Mass\ ratio\ \mu\ (\%)$													
	-	0.1	0.3	0.5	0.6	0.75	1	1.5	2	3	5	7	10	
	-	10.234	7.574	5.802	5.169	4.438	3.610	2.688	2.152	1.454	0.671	0.299	0.091	

* Optimal TMDI configuration ϕ_n^* corresponds actually to TMD (inertance under optimal design is zero)

Table II: Performance ratio $J(\phi_s^* | \theta) / J(\phi_n^* | \theta)$ of optimal simplified design ϕ_s^* over optimal nominal design ϕ_n^* , and optimal inertance ratios β (%) in parenthesis.

TMDI with topologies defined through i_d, i_b														
i_d	i_b	μ (%)												
		TID ($\mu=0$)	0.1	0.3	0.5	0.6	0.75	1	1.5	2	3	5	7	10

10	9	1.34 (269.3)	1.35 (268.3)	1.36 (268.1)	1.09 (268.1)	1.04 ⁺ (0.0)	1.01 ⁺ (0.0)	1.01 ⁺ (0.0)	1.03 ⁺ (0.0)	1.07 ⁺ (0.0)	1.04 ⁺ (0.0)	1.02 ⁺ (0.0)	1.04 ⁺ (0.0)	1.05 ⁺ (0.0)
10	8	2.07 (135.4)	2.10 (135.7)	2.15 (135.7)	2.21 (135.7)	2.23 (135.8)	2.57 (136.6)	2.50 (136.8)	2.51 (137.7)	2.70 (138.1)	2.99 (131.3)	4.28 (132.7)	1.09 ⁺ (0.0)	1.05 ⁺ (0.0)
9	8	2.17 (250.0)	2.17 (252.6)	2.23 (266.4)	2.26 (268.2)	2.27 (268.3)	2.29 (268.5)	2.32 (268.4)	2.34 (262.6)	2.46 (268.3)	2.61 (268.5)	3.72 (268.5)	1.06 ⁺ (0.0)	1.03 ⁺ (0.0)
9	7	6.76 (134.1)	6.84 (136.0)	6.95 (132.9)	7.09 (136.6)	7.24 (128.6)	7.29 (127.0)	7.22 (125.4)	7.77 (121.7)	8.13 (138.9)	8.97 (138.9)	9.57 (126.5)	11.51 (120.4)	18.44 (120.4)
8	7	3.63 (250.0)	3.66 (268.5)	3.70 (268.5)	3.73 (268.5)	3.75 (268.5)	3.77 (268.5)	3.82 (268.5)	3.90 (268.5)	3.95 (254.1)	4.10 (250.0)	4.50 (268.5)	4.86 (262.3)	5.64 (268.5)
8	6	6.56 (157.5)	6.61 (157.6)	6.72 (157.6)	6.85 (157.6)	6.89 (157.3)	6.97 (158.1)	7.10 (157.4)	7.43 (151.2)	7.68 (157.1)	8.14 (151.2)	9.42 (151.2)	10.43 (145.7)	12.16 (140.9)
7	6	1.87 (333.3)	1.87 (333.2)	1.88 (333.5)	1.88 (334.0)	1.88 (334.0)	1.88 (335.4)	1.88 (335.4)	2.06 (327.9)	2.04 (329.3)	2.13 (327.5)	2.23 (329.3)	2.43 (327.4)	2.52 (334.0)
7	5	1.45 (176.1)	1.46 (176.0)	1.39 (180.0)	1.50 (177.3)	1.51 (177.3)	1.44 (180.0)	1.41 (188.3)	1.49 (187.6)	1.68 (180.0)	1.75 (182.1)	2.20 (178.0)	2.59 (175.9)	3.29 (176.0)
1	0	1.86 (395.1)	1.86 (395.0)	1.86 (395.8)	1.88 (395.4)	1.88 (395.6)	1.90 (395.2)	1.87 (397.1)	1.93 (395.0)	1.96 (395.8)	2.07 (391.6)	2.11 (395.1)	2.16 (397.4)	2.32 (397.8)
TMD at top floor														
		μ (%)												
		-	0.1	0.3	0.5	0.6	0.75	1	1.5	2	3	5	7	10
		-	1.19	1.18	1.09	1.04	1.01	1.01	1.06	1.07	1.06	1.02	1.02	1.05

⁺ Optimal TMDI configuration ϕ^* yields a TMD (inertance under optimal design is zero)

Table III: Optimal performance $J(\phi^*)$ [%] for the *robust-exc* case and optimal inertance ratios β (%) in parenthesis.
TMDI with topologies defined through i_d, i_b

i_d	i_b	μ (%)												
		TID ($\mu=0$)	0.1	0.3	0.5	0.6	0.75	1	1.5	2	3	5	7	10
10	9	6.962 (198.0)	6.917 (197.1)	6.817 (194.6)	6.417 (192.3)	5.856 ⁺ (0.0)	5.059 ⁺ (0.0)	4.119 ⁺ (0.0)	3.026 ⁺ (0.0)	2.395 ⁺ (0.0)	1.622 ⁺ (0.0)	0.792 ⁺ (0.0)	0.390 ⁺ (0.0)	0.144 ⁺ (0.0)
10	8	1.853 (103.9)	1.833 (104.0)	1.791 (103.3)	1.749 (101.4)	1.729 (100.8)	1.699 (99.8)	1.649 (98.1)	1.553 (94.1)	1.462 (89.9)	1.291 (81.4)	0.792 ⁺ (0.0)	0.390 ⁺ (0.0)	0.144 ⁺ (0.0)
9	8	2.812 (210.2)	2.797 (209.2)	2.765 (206.9)	2.733 (204.6)	2.718 (203.4)	2.695 (201.7)	2.657 (198.8)	2.583 (192.7)	2.511 (186.5)	1.954 ⁺ (0.0)	1.175 ⁺ (0.0)	0.739 ⁺ (0.0)	0.378 ⁺ (0.0)
9	7	0.475 (135.3)	0.474 (134.3)	0.470 (129.1)	0.467 (130.1)	0.466 (128.7)	0.463 (126.9)	0.459 (125.3)	0.451 (119.7)	0.443 (116.5)	0.426 (108.9)	0.388 (88.2)	0.334 (51.9)	0.214 (24.6)
8	7	1.529 (238.7)	1.526 (237.7)	1.518 (235.6)	1.510 (233.8)	1.506 (232.8)	1.501 (231.4)	1.491 (229.0)	1.473 (224.5)	1.455 (219.7)	1.420 (209.9)	1.352 ⁺ (187.3)	1.291 ⁺ (0.0)	0.951 ⁺ (0.0)
8	6	0.312 (160.4)	0.312 (159.5)	0.3111 (158.2)	0.311 (156.4)	0.311 (155.1)	0.311 (154.8)	0.311 (151.9)	0.310 (146.7)	0.309 (146.4)	0.307 (140.1)	0.303 (127.5)	0.296 (111.6)	0.276 (75.0)
7	6	1.457 (313.3)	1.454 (312.8)	1.447 (312.0)	1.441 (311.1)	1.437 (310.6)	1.432 (310.1)	1.424 (309.0)	1.408 (306.9)	1.392 (304.8)	1.362 (300.4)	1.305 (291.3)	1.254 (280.3)	1.187 (258.1)
7	5	0.168 (184.1)	0.167 (184.4)	0.167 (184.1)	0.166 (184.2)	0.165 (184.0)	0.165 (184.0)	0.164 (183.9)	0.162 (182.4)	0.160 (181.8)	0.157 (180.6)	0.153 (177.8)	0.151 (173.6)	0.151 (165.6)
1	0	0.436 (471.5)	0.436 (471.4)	0.435 (472.0)	0.435 (472.6)	0.434 (472.7)	0.434 (473.3)	0.433 (473.6)	0.432 (474.5)	0.430 (476.1)	0.428 (478.2)	0.422 (483.0)	0.418 (488.0)	0.411 (495.8)
TMD at top floor														
		μ (%)												
		-	0.1	0.3	0.5	0.6	0.75	1	1.5	2	3	5	7	10
		-	10.839	8.328	6.528	5.856	5.059	4.120	3.026	2.395	1.622	0.792	0.390	0.144

⁺ Optimal TMDI configuration ϕ^* yields a TMD (inertance under optimal design is zero)

Table IV: Optimal performance $J(\phi^*)$ [%] for the *robust-full* case and optimal inertance ratios β (%) in parenthesis.

TMDI with topologies defined through i_d, i_b														
i_d	i_b	μ (%)												
		TID ($\mu=0$)	0.1	0.3	0.5	0.6	0.75	1	1.5	2	3	5	7	10
10	9	11.032 (176.5)	10.986 (175.3)	10.883 (172.5)	10.257 (169.5)	9.487 ⁺ (0.0)	8.539 ⁺ (0.0)	7.357 ⁺ (0.0)	5.810 ⁺ (0.0)	4.814 ⁺ (0.0)	3.505 ⁺ (0.0)	2.033 ⁺ (0.0)	1.269 ⁺ (0.0)	0.712 ⁺ (0.0)
10	8	4.479 (100.5)	4.447 (99.9)	4.376 (98.2)	4.308 (97.0)	4.275 (97.2)	4.222 (95.0)	4.138 (93.7)	3.977 (90.9)	3.818 (87.2)	3.509 (77.2)	2.033 ⁺ (0.0)	1.269 ⁺ (0.0)	0.712 ⁺ (0.0)
9	8	5.465 (198.5)	5.446 (197.7)	5.403 (195.7)	5.360 (193.8)	5.339 (192.9)	5.307 (191.4)	5.255 (188.9)	5.152 (184.0)	5.050 (178.9)	4.110 ⁺ (0.0)	2.755 ⁺ (0.0)	1.977 ⁺ (0.0)	1.299 ⁺ (0.0)
		1.534	1.531	1.525	1.518	1.514	1.509	1.501	1.484	1.466	1.431	1.355	1.256	0.973

9	7	(130.2)	(129.3)	(127.7)	(126.0)	(125.5)	(124.3)	(122.8)	(119.7)	(116.8)	(110.9)	(96.5)	(72.0)	(16.9)
8	7	3.087 (238.8)	3.082 (237.7)	3.073 (235.6)	3.063 (233.6)	3.058 (232.5)	3.051 (231.0)	3.039 (228.7)	3.015 (223.8)	2.991 (219.2)	2.943 (209.9)	2.845 (190.0)	2.737 (166.1)	2.443 ⁺ (0.0)
8	6	1.042 (162.0)	1.042 (161.2)	1.042 (159.7)	1.042 (158.3)	1.042 (157.8)	1.042 (156.7)	1.042 (155.5)	1.042 (152.6)	1.041 (150.3)	1.040 (145.4)	1.037 (136.0)	1.029 (125.2)	1.005 (102.1)
7	6	3.163 (331.3)	3.160 (330.8)	3.153 (329.6)	3.145 (328.5)	3.142 (327.8)	3.136 (327.0)	3.127 (325.6)	3.110 (322.9)	3.092 (320.2)	3.056 (315.1)	2.988 (304.9)	2.923 (294.4)	2.833 (276.9)
7	5	0.849 (184.4)	0.849 (185.1)	0.847 (184.8)	0.846 (184.2)	0.846 (184.2)	0.845 (183.9)	0.844 (184.0)	0.841 (182.6)	0.838 (182.1)	0.834 (180.5)	0.828 (178.0)	0.826 (175.4)	0.826 (170.7)
1	0	1.139 (514.6)	1.138 (514.7)	1.138 (515.1)	1.137 (515.4)	1.136 (515.8)	1.135 (516.1)	1.134 (516.6)	1.132 (517.5)	1.129 (518.3)	1.125 (520.4)	1.116 (524.9)	1.107 (528.8)	1.096 (534.3)
TMD at top floor														
		μ (%)												
		-	0.1	0.3	0.5	0.6	0.75	1	1.5	2	3	5	7	10
		-	14.804	12.228	10.258	9.488	8.539	7.349	5.809	4.815	3.509	2.033	1.269	0.712

⁺ Optimal TMDI configuration ϕ^* yields a TMD (inertance under optimal design is zero)

Table V: Performance ratio $J(\phi_n^*) / J(\phi^*)$ of optimal nominal design, ϕ_n^* , under uncertainty to excitation and structural model parameters (note: $J(\phi_n^*) \neq J(\phi_n^* | \theta)$ over *robust-full* design ϕ^*).

TMDI with topologies defined through i_d, i_b														
i_d	i_b	μ (%)												
		TID ($\mu=0$)	0.1	0.3	0.5	0.6	0.75	1	1.5	2	3	5	7	10
10	9	1.01	1.01	1.01	1.02	1.02 ⁺	1.01 ⁺	1.01 ⁺	1.02 ⁺	1.04 ⁺	1.08 ⁺	1.42 ⁺	1.45 ⁺	1.20 ⁺
10	8	1.01	1.01	1.01	1.01	1.01	1.01	1.01	1.01	1.01	1.02	1.42 ⁺	1.45 ⁺	1.20 ⁺
9	8	1.00	1.00	1.00	1.00	1.00	1.00	1.00	1.00	1.00	1.08 ⁺	1.04 ⁺	1.06 ⁺	1.11 ⁺
9	7	1.00	1.00	1.00	1.00	1.00	1.00	1.00	1.00	1.00	1.00	1.00	1.00	1.06
8	9	1.00	1.00	1.00	1.00	1.00	1.00	1.00	1.01	0.91	1.00	1.03 ⁺	1.04 ⁺	1.05 ⁺
8	6	1.01	1.01	1.01	1.01	1.01	1.01	1.01	1.01	1.01	1.02	1.02	1.02	1.01
7	6	1.00	1.00	1.00	1.00	1.00	1.00	1.00	1.00	1.00	1.00	1.00	1.00	1.01
7	5	1.01	1.01	1.01	1.01	1.01	1.01	1.01	1.01	1.00	1.00	1.00	1.00	1.00
1	0	1.03	1.04	1.04	1.03	1.04	1.04	1.02	1.04	1.03	1.03	1.03	1.04	1.04
TMD at top floor														
		μ (%)												
		-	0.1	0.3	0.5	0.6	0.75	1	1.5	2	3	5	7	10
		-	1.00	1.00	1.01	1.02	1.01	1.01	1.02	1.04	1.08	1.42	1.45	1.20

⁺ Optimal TMDI configuration ϕ^* yields a TMD (inertance under optimal design is zero)